Title

Ubiquitin ligase and signalling hub MYCBP2 is required for efficient EPHB2 tyrosine kinase receptor function

Authors

Chao Chang[1,2], Sara L. Banerjee[1,3], Sung Soon Park[1,2], Xiaolei Zhang[1], David Cotnoir-White[1,%], Muriel Desbois[4,5], Brock Grill[4,6,7], and Artur Kania[1,2,3,8,#,*]

Affiliations

[1]Institut de recherches cliniques de Montréal (IRCM), Montréal, QC, H2W 1R7, Canada
[2]Integrated Program in Neuroscience, McGill University, Montréal, QC, H3A 2B4, Canada
[3]Division of Experimental Medicine, McGill University, Montréal, QC, H3A 2B2, Canada
[4]Center for Integrative Brain Research, Seattle Children's Research Institute, Seattle, WA 98101, USA.
[5]School of Life Sciences, Keele University, Keele, Staffordshire ST5 5BG, UK
[6]Department of Pediatrics, University of Washington School of Medicine, Seattle, WA 98101, USA
[7]Department of Pharmacology, University of Washington School of Medicine, Seattle, WA 98195, USA.
[8]Department of Anatomy and Cell Biology, McGill University, Montréal, QC, H3A 0C7, Canada

[%]Current address: Modulari-T Biosciences, Montreal, QC, Canada H4B 1R6

[#]Lead contact
*Correspondence: artur.kania@ircm.qc.ca

Running Title

MYCBP2 functions in EPHB2 signalling.

Abstract

Eph receptor tyrosine kinases participate in a variety of normal and pathogenic processes during development and throughout adulthood. This versatility is likely facilitated by the ability of Eph receptors to signal through diverse cellular signalling pathways: primarily by controlling cytoskeletal dynamics, but also by regulating cellular growth, proliferation, and survival. Despite many proteins linked to these signalling pathways interacting with Eph receptors, the specific mechanisms behind such links and their coordination remain to be elucidated. In a proteomics screen for novel EPHB2 multi-effector proteins, we identified human MYC binding protein 2 (MYCBP2 or PAM or Phr1). MYCBP2 is a large signalling hub involved in diverse processes such as neuronal connectivity, synaptic growth, cell division, neuronal survival, and protein ubiquitination. Our biochemical experiments demonstrate that the formation of a complex containing EPHB2 and MYCBP2 is facilitated by FBXO45, a protein known to select substrates for MYCBP2 ubiquitin ligase activity. Formation of the MYCBP2-EPHB2 complex does not require EPHB2 tyrosine kinase activity and is destabilised by binding of ephrin-B ligands, suggesting that the MYCBP2-EPHB2 association is a prelude to EPHB2 signalling. Paradoxically, the loss of MYCBP2 results in increased ubiquitination of EPHB2 and a decrease of its protein levels suggesting that MYCBP2 stabilises EPHB2. Commensurate with this effect, our cellular experiments reveal that MYCBP2 is essential for efficient EPHB2 signalling responses in cell lines and primary neurons. Finally, our genetic studies in *C. elegans* provide *in vivo* evidence that the ephrin receptor VAB-1 functions within the MYCBP2 signalling network. Together, our results align with the similarity of neurodevelopmental phenotypes caused by MYCBP2 and EPHB2 loss of function, and our findings couple EPHB2 to a signaling effector controlling diverse cellular functions.

Introduction

Eph receptor tyrosine kinases and their membrane-tethered ligands, the ephrins, elicit short distance cell-cell signals that regulate many biological processes. Ephrin-Eph signalling primarily impacts the cytoskeleton with the immobilization of highly dynamic axonal growth cones being a classic example. Other processes that involve changes in transcription, growth, and survival such as angiogenesis, synaptic plasticity, stem cell fate, tumorigenesis and neurodegeneration also involve the Eph/ephrin system. Many proteins are postulated to couple Eph receptors to different intracellular effectors, but the molecular logic of this diversity remains fragmented (Bush, 2022; Kania and Klein, 2016).

EphB subfamily members preferentially bind transmembrane ephrin-Bs and although both molecules participate in bidirectional signalling, ephrin-B activation of EphB signalling cascades is more thoroughly studied (Gale et al., 1996; Mellitzer et al., 1999). To elicit robust Eph receptor forward signalling, ephrins multimerise in signalling clusters by intercalating with Ephs on a signal-recipient cell with array size correlating with signal amplitude (Kullander et al., 2001; Schaupp et al., 2014). Signalling initiation involves the activation of the receptor tyrosine kinase and phosphorylation of tyrosines proximal to the EphB transmembrane domain (Binns et al., 2000; Soskis et al., 2012). Eph-evoked cytoskeletal effects such as cell contraction and growth cone collapse result from changes in small GTPase activity modulated by EphB Guanine nucleotide exchange factors (GEFs) and GTPase activating proteins (GAPs) (Margolis et al., 2010; Shi et al., 2007). Eph signalling has also been linked to fundamental cellular pathways such as the Ras-MAPK pathway, mTOR-regulated protein synthesis, cell division and survival (Bush and Soriano, 2010; Depaepe et al., 2005; Fawal et al., 2018; Genander et al., 2009; Nie et al., 2010). Eph forward signalling eventually leads to their internalisation and either recycling or degradation via endosome/lysosome and ubiquitination/proteasome pathways (Okumura et al., 2017; Zimmer et al., 2003). While identification of a growing number of proteins interacting with Eph receptors has moved the field forward, we have yet to clarify the question of how Eph receptors activate various fundamental cellular processes, often within the same cell type.

Myc-binding protein 2 (MYCBP2), also known as Highwire, RPM-1, Protein Associated with Myc (PAM) and Phr1, is a large signalling hub that regulates cytoskeletal dynamics, neuronal development, and axonal degeneration (Guo et al., 1998, Grill et al., 2016; Virdee, 2022). It has an atypical RING ubiquitin ligase activity that inhibits the p38/MAP and JNK kinase pathways thereby regulating cytoskeletal dynamics underlying axonal development and synaptic growth (Borgen et al., 2017; Collins et al., 2006; Lewcock et al., 2007; Nakata et al., 2005; Pao et al., 2018; Wan et al., 2000). MYCBP2 further regulates the Tuberin Sclerosis Complex linked to cell growth (TSC; (Han et al., 2012)), initiation of autophagy via ULK (Crawley et al., 2019) and NMNAT2-regulated neuronal survival and axonal degeneration (Babetto et al., 2013; Xiong et al., 2012). Biochemical mapping has shown that human MYCBP2 and its *C. elegans* ortholog

RPM-1 rely upon the FBD1 domain to bind the F-box protein FBXO45 that acts as a ubiquitination substrate selector (Desbois et al., 2018); (Sharma et al., 2014). Intriguingly, the neurodevelopmental phenotypes caused by MYCBP2 and EPHB2 loss of function are similar, raising the possibility that these two molecules could function in the same pathway (Dalva et al., 2000; Henkemeyer et al., 1996; Lewcock et al., 2007). Nonetheless, a biochemical or genetic interaction between MYCBP2 and EPHB2 has not been demonstrated in any system.

To shed light on how EphB receptors fulfil their multitude of functions, we used mass spectrometry (MS)-based proteomics to identify multi-effector proteins that bind EPHB2. One of our proteomic hits was MYCBP2, which we demonstrated forms a complex with EPHB2 using a combination of biochemical and cellular assays. Furthermore, we show that this interaction is required for efficient EPHB2 signalling in cell lines and primary neurons. Consistent with these findings, we observed *in vivo* genetic interactions between the Eph receptor, VAB-1, and the RPM-1 signalling network in the nervous system of *C. elegans*. Our collective results indicate that the relationship between EPHB2 and MYCBP2 does not appear to involve the ubiquitin ligase activity of MYCBP2, and raise the possibility that MYCBP2 links EPHB2 to diverse fundamental cellular functions.

Results

Proteomics identifies MYCBP2 as a putative EPHB2-interacting protein

To understand the molecular logic underlying EPHB2 signalling diversity, we performed affinity purification coupled to MS (AP-MS) in order to identify EPHB2-interacting proteins, and prioritised those known to be signalling hubs. We used a stable HeLa cell line with tetracycline-inducible expression of BirA-linked EPHB2-FLAG, that we previously used to study EPHB2 signalling (Lahaie et al., 2019). To identify ephrin ligand-dependent EPHB2 protein complexes, we stimulated EPHB2-FLAG-overexpressing cells with pre-clustered Fc control or ephrinB2-Fc (eB2-Fc). We then harvested and lysed the cells, performed anti-FLAG immunoprecipitation, and used mass spectrometry to identify EPHB2 protein complexes (Fig. 1A).

To identify EPHB2-specific interactions and remove background contaminants, we performed Significance Analysis of INTeractome (SAINTexpress analysis (Teo et al., 2014)) using our EPHB2-related controls (Lahaie et al., 2019). To better visualize the changes in putative EPHB2 binding partners, we compared the average spectral counts of the identified proteins using ProHits-viz tool (Knight et al., 2017). Comparison of Fc and ephrin-B2-treated samples did not yield any significant differences. Since we applied the ligand and collected the samples on a time scale comparable to known EphB signalling dynamics, this limitation could be potentially due to autoactivation of Eph receptors when they are overexpressed, obscuring some ligand-dependent effects (Lackmann et al., 1998). However, the resulting scatter plot confirmed the presence of several known EPHB2 interactors, such as FYN and YES1 Src kinases and members of the Eph receptor family (Fig. 1B) (Banerjee et al., 2022). One of the most prominent, novel hits was the E3 ubiquitin ligase and signalling hub protein MYCBP2, and its binding partner FBXO45. FBXO45 was previously identified as a putative EPHB2 interacting protein in large-scale, cell-based interactome studies (Huttlin et al., 2021; Salokas et al., 2022).

Biochemical validation of MYCBP2 binding to EPHB2

To confirm that MYCBP2 can indeed form a molecular complex with EPHB2, we tested whether endogenous MYCBP2 co-immunoprecipitates (co-IP) with FLAG-tagged EPHB2 in HEK 293T cells. Based on differences in EPHB2 and EPHA3 interactomes, we reasoned that EPHA3 may serve as a negative control for the EPHB2-MYCBP2 association (Huttlin et al., 2021). We found that MYCBP2 coprecipitated with affinity-purified EPHB2-FLAG, but not EPHA3 (Fig. 1C). This confirmed MYCBP2 binding to EPHB2 and suggested MYCPB2 displays EPH receptor subtype specificity. Importantly, the EPHB2-MYCBP2 interaction was reduced by 24.5% and 53% following ephrin-B1 and ephrin-B2 treatment respectively in HeLa EPHB2 cells, suggesting the involvement of MYCBP2 in ephrin-B:EPHB2 signalling (Fig. 1D, E, eB1-Fc, p=0.1365; eB2-Fc,

p=0.0002). To test this interaction *in vivo*, we performed co-IP from rat brain, which further confirmed MCYBP2 association with EPHB2 (Fig. 1F).

We next asked whether the kinase activity of EPHB2 is required for the formation of the EPHB2-MYCBP2 complex. To test this, we expressed GFP-tagged wild type (WT) EPHB2 or EPHB2 with a kinase-dead mutation (KD) in HeLa cells. We found that MYCBP2 showed comparable coprecipitation with WT and KD EPHB2 (Fig. 1G). Thus, EPHB2 kinase activity is not required for the formation of MYCBP2 - EPHB2 complexes, suggesting that MYCBP2 association with EPHB2 may be a prelude to ephrin-B-evoked EPHB2 signalling.

FBXO45 enhances the association between MYCBP2 and EPHB2

Our proteomics screen for EPHB2 interactors also identified FBXO45, the F-box protein that forms a ubiquitin ligase complex with MYCBP2 (Saiga et al., 2009; Sharma et al., 2014). Thus, we initially reasoned that FBXO45 might perform a similar role in the formation of the MYCBP2-EPHB2 complex. We first tested whether FBXO45 binds to EPHB2 by co-expressing MYC-tagged FBXO45 with EPHB2-FLAG or EPHA3-FLAG in HEK293T cells. Co-IP revealed that FBXO45 can associate with EPHB2 but not EPHA3, suggesting that EPHB2, FBXO45 and MYCBP2 could form a ternary complex (Fig. 2A). To test this idea, we co-expressed EPHB2-FLAG and GFP-MYCBP2 in the presence or absence of MYC-FBXO45 and examined co-IP efficiency between EPHB2 and MYCBP2. Interestingly, FBXO45 enhanced the interaction between EPHB2 and MYCBP2 (Fig. 2B). Together, these data suggest that EPHB2 can form a complex with both MYCBP2 and FBXO45, and that FBXO45 increases the efficiency of MYCBP2-EPHB2 interaction.

Biochemical mapping of EPHB2-MYCBP2 interaction

To identify the MYCBP2 protein domain(s) required for the formation of the ternary complex with EPHB2 and FBXO45, we co-expressed EPHB2-FLAG and three GFP-MYCBP2 fragments in HEK293T cells. Co-IP revealed that the central region of MYCBP2 was sufficient for binding with EPHB2 (Fig. 2C, D). In addition, co-expression of MYC-FBXO45 demonstrated that the association of the central domain of MYCBP2 with EPHB2 is enhanced by FBOX45 and is consistent with the presence of an FBXO45 binding site within this MYCBP2 fragment (Fig. 2D) (Sharma et al., 2014).

To identify the domains of EPHB2 required for the formation of the tripartite complex, we took advantage of the observation that EPHA3 does not readily form a complex with MYCBP2 or FBXO45. Thus, we performed domain swapping experiments between EPHB2 and EPHA3

197 reasoning that placing EPHA3-specific sequences in EPHB2 would inhibit the formation of the
198 tripartite complex. We constructed a series of FLAG-EPHB2/EPHA3 chimeras and determined
199 whether they bound MYCBP2 in the presence of FBXO45 (Fig. 2E). Co-IP revealed that the
200 ability of a particular chimera to associate with MYCBP2 was correlated with its association with
201 FBXO45, in line with the MYCBP2-FBXO45 complex interacting with EPHB2. Surprisingly, we
202 found that EPHB2-EPHA3 chimeras with an EPHA3 identity of intracellular juxtamembrane,
203 kinase, SAM or PDZ binding domains retained the ability to associate with FBXO45 and
204 MYCBP2, suggesting that the formation of the tripartite complex is driven by the extracellular
205 domain and/or the transmembrane domain of EPHB2 (Fig. 2F). However, these results are also
206 consistent with the possibility that the EPHB2 identity of the extracellular fragments could alter
207 the conformation of the intracellular domains of EPHA3 identity, allowing the interaction with
208 FBXO45-MYCBP2 to occur. To exclude this possibility, we created EPHB2 mutants lacking the
209 intracellular or extracellular domains and tested their ability to complex with MYCBP2 and
210 FBXO45 by co-IP (Fig. 2G). In these experiments only the deletion mutant lacking the
211 intracellular domain retained its ability to form the tripartite complex. Collectively, these results
212 argue that the combination of extracellular and transmembrane domains of EPHB2 are
213 necessary and sufficient for formation of the MYCBP2–FBXO45–EPHB2 complex (Fig. 2H).
214
215
216 **MYCBP2 is required for EPHB2-mediated cellular responses**
217
218 Given the decrease in MYCBP2–EPHB2 association evoked by ephrin-B treatment (Fig. 1D, E),
219 we next sought to determine whether MYCBP2 fulfils a specific function in ephrin-B:EPHB2
220 forward signalling. Thus, we used EPHB2-FLAG HeLa cells to generate a *MYCBP2*^{CRISPR} HeLa
221 cell line, which stably integrated CRISPR sgRNA targeting the *MYCBP2* exon 6 using lentivirus
222 (Desbois et al., 2018). Using EPHB2-FLAG HeLa cells carrying a stably integrated empty
223 expression vector (CTRL^{CRISPR}) as controls, we found that *MYCBP2*^{CRISPR} led to a reduction in
224 endogenous MYCBP2 protein levels (Fig. 3A).
225
226 To study the role of MYCBP2 in EphB signalling, we took advantage of an experimental
227 paradigm in which exposure to ephrin-B2 evokes cytoskeletal contraction of HeLa cells
228 expressing EPHB2 (Lahaie et al., 2019). Thus, following induction of EPHB2 expression,
229 *MYCBP2*^{CRISPR} and CTRL^{CRISPR} cells were stimulated with pre-clustered Fc control or ephrin-B2
230 for 15 minutes and scored as collapsed or uncollapsed. While the proportion of collapsed cells
231 for the two cell lines treated with Fc was similar (CTRL^{CRISPR}, 5.4%; *MYCBP2*^{CRISPR}, 5.7%;
232 p=0.9841), ephrin-B2 treatment resulted in the collapse of 19.0% of CTRL^{CRISPR} cells but only
233 12.1% of *MYCBP2*^{CRISPR} cells (n=9 coverslips; Fig. 3B, C; p=0.0017). In addition, time-lapse
234 imaging of *MYCBP2*^{CRISPR} and CTRL^{CRISPR} cells transiently transfected with an EPHB2-GFP
235 expression plasmid revealed a similar attenuation of ephrin-B2-induced cellular contraction (Fig.

236 3D, E; p=0.0268). These data argue that MYCBP2 regulates a short-term cellular response
237 evoked by ephrin-B2:EPHB2 signalling.
238
239 To study longer-term cellular responses evoked by ephrin-B2:EPHB2 signalling, we
240 turned to a stripe assay in which the preference of CTRL^{CRISPR} and *MYCBP2*^{CRISPR} cells for
241 immobilized ephrin-B2 or Fc was measured. To do this, cells of either line were deposited over
242 alternating stripes of ephrin-B2 or Fc, and stripe preference was scored for individual cells after
243 overnight incubation. While only 33.2% of CTRL^{CRISPR} cells resided on ephrin-B2 stripes, this
244 proportion was significantly increased to 47.4% for *MYCBP2*^{CRISPR} cells, suggesting the loss of
245 MYCBP2 function led to a decreased repulsion from ephrin-B2 stripes (Fig. 3F, G; n=5 and 7
246 carpets respectively, p=0.0109). Together, our data suggest that MYCBP2 is required for
247 EPHB2-mediated cellular responses in HeLa cells.
248
249
250 **Loss of MYCBP2 decreases cellular levels of EPHB2 protein**
251
252 The association of EPHB2 with MYCBP2 and its substrate recognition protein FBXO45 suggests
253 that the MYCBP2 ubiquitin ligase complex could target EPHB2 for degradation, a mechanism
254 frequently deployed to terminate transmembrane receptor signalling (Foot et al., 2017). However,
255 the results of our cellular assays contradicted this model, and rather suggested that loss of
256 MYCBP2 function decreased EPHB2 signalling. To further evaluate these two scenarios, we first
257 compared tetracycline-induced levels of EPHB2 protein in HeLa *MYCBP2*^{CRISPR} cells and
258 CTRL^{CRISPR} cells. We found that impairing MYCBP2 reduced EPHB2 protein levels (Fig. 4A). To
259 extend our data, we transfected EPHB2-FLAG into both CTRL^{CRISPR} and *MYCBP2*^{CRISPR} cells
260 and examined EPHB2-FLAG levels after two days. As shown in Fig. 4B, C, levels of EPHB2-
261 FLAG were significantly lowered by 26.1% in HeLa *MYCBP2*^{CRISPR} cells compared to
262 CTRL^{CRISPR} cells (p=0.0046). We further investigated whether MYCBP2 affects EPHB2 protein
263 turnover when cycloheximide is added to prevent new protein synthesis. EPHB2-FLAG
264 expression was induced by tetracycline for 12 hours followed by protein synthesis inhibition with
265 cycloheximide. We found that EPHB2 half-life was reduced in HeLa cells lacking MYCBP2
266 compared to control (Fig. 4D, E; 8h treatment, p=0.0474).
267
268 Ephrin ligand treatment eventually results in Eph receptor degradation, a process
269 associated with signalling termination. We therefore asked whether ligand-mediated EPHB2
270 receptor degradation depends on MYCBP2. We induced EPHB2 expression in CTRL^{CRISPR} and
271 *MYCBP2*^{CRISPR} cells, and exposed them to ephrin-B2 for a different length of time. Western
272 blotting revealed that 4-8 hours stimulation with ephrin-B2 reduced EPHB2 levels in CTRL^{CRISPR}
273 cells, but this effect was more drastic in *MYCBP2*^{CRISPR} cells (Fig. 4F, G). Taken together, our
274 results are not consistent with MYCBP2 ubiquitinating EPHB2 and causing its degradation.

Unexpectedly, our data indicate that MYCBP2 stabilizes EPHB2 in HeLa cells under both naïve and ligand-challenged conditions.

Loss of MYCBP2 enhances ligand-induced EPHB2 receptor ubiquitination

Ubiquitination of receptor tyrosine kinases, including Eph receptors, can herald their degradation via the proteasome and thus termination of signalling (Haglund and Dikic, 2012; Sabet et al., 2015). This model is not supported by our results, which suggest that MYCBP2 is required for EPHB2 protein maintenance. Nonetheless, we investigated whether EPHB2 receptor ubiquitination is altered in HeLa cells depleted of MYCBP2. HeLa CTRL^{CRISPR} and *MYCBP2*^{CRISPR} cells were transfected with HA-tagged ubiquitin, EPHB2 expression was induced with tetracycline, and cells were treated with ephrin-B2 for 30min. We observed that EPHB2 receptor ubiquitination was not significantly increased in CTRL^{CRISPR} cells after this short-term ligand treatment (Fig. 4H, I CTRL^{CRISPR}, p=0.1349). In contrast, EPHB2 ubiquitination was significantly increased in *MYCBP2*^{CRISPR} cells (Fig. 4H, I *MYCBP2*^{CRISPR}, p=0.0195). This effect argues against the concept that EPHB2 is a MYCBP2 ubiquitination substrate, and suggests that in the absence of MYCBP2 degradation of the EPHB2 receptor is enhanced due to increased ubiquitination.

Loss of MYCBP2 promotes EPHB2 degradation through the lysosomal pathway

EPHB2 can be degraded by either a proteasomal or lysosomal pathway depending on the cellular context (Cissé et al., 2011; Fasen et al., 2008; Litterst et al., 2007). Thus, we wanted to shed light on how EPHB2 is degraded and understand why EPHB2 degradation is enhanced by MYCBP2 loss of function. To do so, we induced EPHB2 expression in CTRL^{CRISPR} and *MYCBP2*^{CRISPR} cells and applied the S26 proteasome inhibitor MG132, or the lysosomal inhibitors BafilomycinA1 or Chloroquine. We found that MG132 did not have significant effects on EPHB2 levels in both cell types (Fig. 4J, K). However, we found that BafilomycinaA1 (BafA1) significantly increased EPHB2 protein levels in both HeLa CTRL^{CRISPR} cells and *MYCBP2*^{CRISPR} cells by 19% and 40%, respectively (Fig. 4J, K). We also observed a trend towards increased EPHB2 levels with Chloroquine (coQ) treatment in CTRL^{CRISPR} (14%) and MYCBP2^{CRISPR} (35%), further suggesting a role for lysosomal degradation (Fig. 4J, K). These observations suggest that the loss of MYCBP2 promotes EPHB2 receptor degradation through the lysosomal pathway, which expands our understanding of how lysosomal degradation of EPHB2 is regulated.

Loss of MYCBP2 does not decrease EPHB1, EPHB3, or EPHA3 receptor levels

The above experiments raise the question of whether MYCBP2 is a general regulator of Eph receptor stability. Since EPHA3 does not form a complex with MYCBP2, and EphA receptor levels are controlled by the proteasomal pathway (Sharfe et al., 2003; Walker-Daniels et al., 2002), we hypothesized that MYCBP2 might regulate the levels of the entire EphB receptor class. To test this, we co-transfected plasmids encoding GFP-tagged EPHB1 and HA-tagged EPHB3 into HeLa CTRL^{CRISPR} and *MYCBP2*^{CRISPR} cells. Compared to CTRL^{CRISPR} cells, EPHB1 and EPHB3 levels were not significantly reduced in *MYCBP2*^{CRISPR} cells (Fig. 4L, M, EPHB1, p=0.0588; EPHB3, p=0.4253). Likewise, FLAG-EPHA3 levels were similar in CTRL^{CRISPR} and *MYCBP2*^{CRISPR} cells (Fig. 4N, O, p=0.5369). Taken together, these data suggest that MYCBP2 specifically affects EPHB2 receptor stability.

Loss of MYCBP2 attenuates the magnitude of EPHB2 cellular signalling

EPHB2 receptor activation evokes signal transduction events such as tyrosine phosphorylation of EPHB2, activation of EPHB2 tyrosine kinase function and phosphorylation of the ERK1/2 downstream effector (Poliakov et al., 2008). We therefore measured EPHB2 and ERK1/2 phosphorylation in CTRL^{CRISPR} and *MYCBP2*^{CRISPR} cells for up to 8 hours after ephrin-B2 application (Fig. 5A). P-EPHB2 (pY20) and p-ERK1/2 signals were normalised to GAPDH and ERK1/2, respectively. In HeLa CTRL^{CRISPR} cells, pTyr-EPHB2 response reached a plateau after 1-2 h treatment and remained up 8 hours post-stimulation (Fig. 5A-C). On the contrary, ephrin-B2-evoked phosphorylation of EPHB2 was reduced in *MYCBP2*^{CRISPR} cells with quantitative results showing a significant reduction by 8 hours of treatment (Fig. 5A, C; 8h p=0.0331). We were also able to detect significantly lower p-ERK1/2 levels in *MYCBP2*^{CRISPR} cells relative to CTRL^{CRISPR} cells, although activation of ERK1/2 by ephrin-B2 was variable (Fig. 5D. 4h, p=0.0494; 8h, p=0.0078; n=6). We again noted significantly enhanced EPHB2 degradation in *MYCBP2*^{CRISPR} cells (Fig. 5E; 8h, p=0.0437). This decrease was also observed when CTRL^{CRISPR} and *MYCBP2*^{CRISPR} cells were treated with ephrin-B1 (data not shown).

Next, we asked whether the decrease in ligand-evoked EPHB1/2 and ERK1/2 activation in *MYCBP2*^{CRISPR} cells reflects a requirement for MYCBP2 in the EPHB2 signalling cascade per se, or whether it is explained by decreased EPHB2 protein levels caused by MYCBP2 loss. We thus normalized p-EPHB2 and p-ERK1/2 signal to the levels of EPHB2 protein at all time points, which revealed that kinetics and magnitude of EPHB2 and ERK1/2 phosphorylation are similar between CTRL^{CRISPR} and *MYCBP2*^{CRISPR} cells (Fig. 5F, G). Although these data argue against a direct role of MYCBP2 in the early events of EPHB2 signalling, they nevertheless indicate that MYCBP2 loss results in marked attenuation of EPHB2 activation and its downstream pERK1/2 signalling in line with decreased cellular responses to ephrin-B2.

355 **Exogenous Fbxo45 binding domain of MYCBP2 disrupts the EPHB2-MYCBP2 interaction**
356
357 Previous studies showed that FBXO45 binds to the FBD1 domain of MYCBP2, and exogenous
358 FBD1 overexpression can disrupt the FBXO45-MYCBP2 association (Sharma et al., 2014). We
359 thus tested whether FBD1 overexpression can interfere with the formation of the EPHB2-
360 MYCBP2 complex (Fig. 6A). Indeed, the expression of GFP-FBD1 wild-type (WT) in HEK cells
361 expressing EPHB2-FLAG and MYC-FBXO45 reduced binding between EPHB2 and MYCBP2
362 (Fig. 6B). This effect was not observed with a GFP-FBD1 mutant (mut) fragment that harbours
363 three point mutations that inhibit binding to FBXO45. Reduction of the EPHB2-MYCBP2
364 interaction was also observed in cells that were not overexpressing FBXO45 (Fig. 6C). Thus,
365 exogenous FBD1 can specifically disrupt the EPHB2-MYCBP2 association. This suggests that
366 FBXO45 binding to MYCBP2 may facilitate for formation of the MYCBP2-EPHB2 complex.
367
368 **FBD1 expression impairs EPHB2-mediated neuronal responses**
369
370 To determine whether the EPHB2-MYCBP2 interaction is required for EPHB2 function, we
371 disrupted binding via FBD1 ectopic expression in cell lines or primary neurons, and studied
372 cellular responses to ephrin-B treatment. We introduced GFP-FBD1 mut or GFP-FBD1 WT into
373 HeLa cells with inducible EPHB2 expression and cultured these cells on ephrin-B2 and Fc stripes.
374 Following overnight culture, only 19.2% of cells expressing GFP-FBD1 mut resided on ephrin-
375 B2 stripes. In contrast, 28.6% of cells expressing GFP-FBD1 WT were found on ephrin-B2
376 stripes indicating that FBD1 expression can dampen ephrin-B2:EPHB2 mediated cell repulsion
377 (Fig. 6D, E; p=0.0107).
378
379 Since EPHB2 is expressed in the embryonic chicken spinal cord, we performed *in ovo*
380 electroporation to introduce plasmids encoding GFP-FBD1 mut or GFP-FBD1 WT into the spinal
381 cords of 2.5-day old embryonic chickens (Hamburger-Hamilton; (HH) Stage 15-17; (Hamburger
382 and Hamilton, 1951; Luria et al., 2008)). Two days later spinal cords were dissected, divided into
383 explants, cultured overnight on alternating stripes containing ephrin-B2 or Fc, and axonal GFP
384 signal present over ephrin-B2 versus Fc stripes was determined. When explants expressed
385 GFP-FBD1 mut (negative control), we observed 26.5% of axonal GFP signal resided on ephrin-
386 B2 stripes (Fig. 7A, B). In contrast, we found a significant increase of 32.2% of neurites
387 expressing FBD1 WT on ephrin-B2 stripes (Fig. 7A, B; p=0.0410). Thus, FBD1 expression
388 impairs long-term repulsive responses to ephrinB2-EPHB2 signalling in spinal explants.
389
390 To study short-term neuronal responses to ephrin-Bs, we turned to mouse hippocampal
391 neurons and a growth cone collapse assay (Srivastava et al., 2013). Here, we electroporated
392 GFP-FBD1 mut or GFP-FBD1 WT expression plasmids into dissociated hippocampal neurons
393 and treated them with pre-clustered Fc, ephrin-B1 or ephrin-B2 for one hour (Fig. 7C). Neurons
394 expressing GFP-FBD1 mut showed 33.9% growth cone collapse with Fc treatment, while Ephrin-

395 B1 and Ephrin-B2 treatment elicited significant increases to 57.9% and 53.3% collapse,
396 respectively (Fig. 7C, D). Importantly, both ephrin-B ligands significantly increased the frequency
397 of growth cone collapse with respect to Fc treatment when FBD1 mut was expressed (Fig. 7D;
398 $p<0.0001$, and $p=0.0008$). In contrast, this effect was either significantly reduced or less evident
399 in neurons expressing GFP-FBD1 WT: with only 48.1% and 57.5% growth cones being collapsed
400 by ephrin-B1 and ephrin-B2, respectively, compared to 41.7% being collapsed by Fc treatment
401 (Fig. 7D; $p=0.4357$ and $p=0.0065$, respectively). Together, these data indicate that impairing
402 MYCBP2 function via FBD1 expression disrupts ephrin:B-EPHB2 signalling in axonal guidance.
403
404
405 ***C. elegans* ephrin receptor VAB-1 interacts genetically with the RPM-1/MYCBP2 signalling**
406 **network**
407
408 Next, we sought to test genetic interactions between an ephrin receptor and the MYCBP2
409 pathway using an *in vivo* animal model. To do so, we turned to *C. elegans* where we evaluated
410 the sole Eph family receptor in this organism, VAB-1, and its genetic relationship with several
411 genes in the MYCBP2 signalling network. *C. elegans* has a single MYCBP2 ortholog called
412 RPM-1, and previous studies have shown that RPM-1/MYCBP2 is required to terminate axon
413 outgrowth (Grill et al., 2016). Previous work showed that axon termination defects in *rpm-1*
414 mutants are due to impaired growth cone collapse (Borgen et al., 2017). Axon termination is also
415 regulated by several downstream players in the RPM-1 signalling network including FSN-
416 1/FBXO45 and GLO-4, a Rab GEF orthologue of human SERGEF (Grill et al., 2007).
417
418 To evaluate genetic interactions between the VAB-1 Eph receptor and RPM-1/MYCBP2
419 signalling, we used the PLM mechanosensory neurons of *C. elegans*. There are two PLM
420 neurons with one on either side of the body. Each PLM neuron extends a primary axon that
421 grows anteriorly and terminates at a precise location before the cell body of another
422 mechanosensory neuron called ALM (Fig. 8A). Consistent with previous studies (Mohamed and
423 Chin-Sang, 2006), *vab-1* loss-of-function (lf) mutants presented moderate axon termination
424 defects where the PLM axon overextends beyond the ALM cell body (Fig. 8A). Quantitation
425 indicated that this phenotype occurred at a low, but significant frequency (Fig. 8B). We then
426 examined the genetic relationship between *vab-1* and the Rab GEF *glo-4*. We observed both
427 moderate overextension defects and more severe defects in which the axon hooked ventrally in
428 *vab-1; glo-4* double mutants (Fig. 8A). The frequency of both types of axon termination defects
429 were significantly enhanced in *vab-1; glo-4* double mutants, and overextension defects were
430 significantly rescued by transgenic expression of VAB-1 (Fig. 8A, B). We subsequently tested
431 the relationship between the Fbox protein *fsn-1* and *vab-1*, and observed enhanced defects in
432 *vab-1; fsn-1* double mutants (Fig. 8C). Finally, we evaluated *vab-1*; *rpm-1* double mutants and
433 did not observe a significant change in phenotypic severity or penetrance compared to *rpm-1*
434 single mutants (Fig. 8D).

Collectively, these genetic experiments support several conclusions. 1) Enhanced defects in *vab-1; glo-4* and *vab-1; fsn-1* double mutants indicate that the VAB-1 Ephrin receptor functions in parallel to known players in the RPM-1 signalling network to facilitate axon termination. 2) The absence of enhanced defects in *vab-1; rpm-1* double mutants indicates that VAB-1 functions in the same genetic pathway as RPM-1. 3) Lack of suppression in *vab-1; fsn-1* and *vab-1; rpm-1* double mutants indicates that VAB-1 is neither ubiquitinated nor inhibited/degraded by the RPM-1/FSN-1 ubiquitin ligase complex. Together, these data from the *C. elegans* model are consistent with our proteomic, biochemical and cellular observations arguing that MYCBP2 binds to EPHB2 to protect it from degradation.

Discussion

Our MS-based proteomics efforts to identify EPHB2 interacting proteins yielded MYCBP2, a signalling hub and ubiquitin ligase that is functionally linked to many of the cellular processes also mediated by EPHB2, including cellular growth, proliferation, synapse formation, and axon development. Our experiments argue against EPHB2 being a MYCBP2 ubiquitination substrate. Instead, we envisage a model where MYCBP2 controls EPHB2 signalling indirectly by preventing its lysosomal degradation and maintaining EPHB2 protein levels sufficiently high to mediate efficient cellular and axonal growth cone repulsion from ephrin-B ligands. The interaction between MYCBP2 and EPHB2 may allow the coupling EPHB2 to fundamental cellular processes that control growth, proliferation, and survival. Here, we discuss the molecular logic of MYCBP2 and EPHB2 association in the context of Eph receptor signalling, its potential implications for neural development and diversification of EphB2 signalling.

Functional significance of MYCBP2-EPHB2 complex formation

Our biochemical experiments validate the formation of a MYCBP2-EPHB2 complex and suggest that this association is decreased following ligand application. Because PHR proteins like MYCBP2 are large signalling hubs, MYCBP2 association with EPHB2 might sterically hinder the formation of EPHB2 multimers and clusters necessary for signalling. Thus, ligand-induced dissociation of the MYCBP2-EPHB2 complex could be a prelude to signalling. Our findings indicate that MYCBP2 association with EPHB2 is enhanced by FBXO45, a subunit of the MYCBP2/FBXO45 complex that mediates ubiquitination substrate binding. Previous work showed that MYCBP2 functions to polyubiquitinate specific protein substrates, targeting them for degradation and inhibition (Crawley et al., 2019; Desbois et al., 2022; Han et al., 2012; Nakata et al., 2005). We considered the possibility that the ubiquitin ligase activity of MYCBP2 is important for the termination of EPHB2 signalling, but several lines of evidence argue against this idea: (1) the application of ephrin-B2 ligand results in the dissociation of the MYCBP2-EPHB2 complex, (2) loss of MYCBP2 function results in decreased cellular levels of EPHB2 protein, and (3) impairing MYCBP2 increases ligand-stimulated EPHB2 ubiquitination. In addition, our quantification of EPHB2 signalling suggested that decreased EPHB2 and ERK phosphorylation seen in MYCBP2-deficient cells can be accounted for by the decrease in EPHB2 receptor levels. Thus, a more plausible model that is consistent with our results is that MYCBP2 association with EPHB2 protects EPHB2 from turnover by lysosome-mediated degradation and prevents EPHB2 ubiquitination by the action of unidentified ubiquitin ligases. Interestingly, studies in *C. elegans* have shown that RPM-1/MYCBP2 regulates lysosome biogenesis (Grill et al., 2007). While this established a link between MYCBP2 signalling and the endo-lysosomal degradation system, our results now indicate that MYCBP2 can also influence turnover of

EPHB2 via lysosomal degradation. Consistent with these findings, we observed that the Eph receptor VAB-1 functions in the RPM-1 signalling network and in a parallel genetic pathway with GLO-4, the RPM-1 binding protein that mediates effects on lysosome biogenesis.

The "protective" effect of MYCBP2 vis-à-vis EPHB2 ubiquitination and lysosomal degradation might be secondary to effects on other aspects of EPHB2 signalling that we have not explored experimentally. For example, since MYCBP2 is a signalling hub with multiple substrates and binding proteins, it could bring EphB2 into close proximity to components of the MYCBP2 signalling network integrating cell-cell communication via ephrin:Eph signals with MYCBP2 intracellular signalling to influence fundamental cellular processes. One example of this is suggested by a recent study demonstrating a link between EPHB2 and mTOR-mediated cell growth signalling pathways (Gagne et al., 2021). One potential mechanism could involve Ephrin binding-induced dissociation of the EPHB2-MYCBP2 interaction, allowing MYCBP2 ubiquitination of the TSC complex that regulates mTOR function (Han et al., 2012).

The formation of a MYCBP2-EPHB2 complex that includes other signalling receptors could also explain the curious result that the extracellular domain of EPHB2 is critical for MYCBP2 association. The finding would be consistent with the extracellular domain of EPHB2 interacting with the extracellular domains of other receptors, whose intracellular domains are linked more directly with MYCBP2 and FBXO45. An alternative explanation may be a non-classical extracellular MYCBP2-EPHB2 interaction similar to the one proposed for the extracellular domain of N-Cadherin and FBXO45 (Na et al., 2020).

MYCBP2 and EPHB2 functions in the developing nervous system

Our proteomic, biochemical, and genetic experiments indicate that MYCBP2 and EPHB2 function in the same pathway. This is also supported by the striking similarity of MYCBP2 and EPHB2 loss of function phenotypes in the mouse nervous system. In the context of developing neuronal connections, *EphB2* and *Mycbp2/Phr1* mouse mutants display similar axon guidance phenotypes such as abnormal limb nerve trajectories by motor axons, defective growth cone crossing of the midline at the level of the optic chiasm and decreased connectivity between the two cortical hemispheres through the corpus callosum (D'Souza et al., 2005; Henkemeyer et al., 1996; Lewcock et al., 2007; Luria et al., 2008; Williams et al., 2003). Both proteins also function in synaptic development and their loss of function leads to decreased numbers of synapses and altered synapse morphology (Bloom et al., 2007; Dalva et al., 2000; Wan et al., 2000; Zhen et al., 2000). Furthermore, outside the nervous system, both are involved in a variety of cancers with recent evidence linking them to esophageal adenocarcinoma and c-MYC-dependent control of cell proliferation (Genander et al., 2009; Han et al., 2012; Venkitachalam et al., 2022). Our

525 proteomic, biochemical, and cellular experiments together with genetic experiments in *C.*
526 *elegans* now provide a new framework in which to consider phenotypic and disease links
527 between EPHB2 and MYCBP2.
528
529 Importantly, the biomedical relevance of our findings are heightened by a recent study
530 that identified genetic variants in MYCBP2, which cause a neurodevelopmental disorder termed
531 *MYCBP2*-related Developmental delay with Corpus callosum Defects (MDCD) (Al-Abdi et al.,
532 2022). MDCD features defective neuronal connectivity including a hypoplastic or absent corpus
533 callosum, neurobehavioral deficits including intellectual disability and epilepsy, and abnormal
534 craniofacial development. This constellation of comorbidities in MDCD closely resembles some
535 of the phenotypes observed in mice with deficient EPHB2 signalling. Given our finding that
536 MYCBP2 loss reduces EPHB2 levels and influences Eph receptor effects on axon development,
537 the question of whether EPHB2 expression levels are normal in MYCBP2 patients remains
538 pertinent.
539
540 In conclusion, our study has revealed numerous biochemical and genetic links between
541 MYCBP2 and EPHB2. Our findings indicate that the MYCBP2/FBXO45 complex protects
542 EPHB2 from degradation, and these are functionally integrated signalling players with an
543 evolutionarily conserved role in axonal development. Future studies will be needed to address
544 how the EPHB2-MYCBP2 interaction affects nervous system development in mammals *in vivo*
545 and to identify further regulators of EPHB2 degradation. Additionally, another idea worthy of
546 closer examination in the future is the possibility that MYCBP2 signalling could provide routes
547 through which EPHB2-initiated signals access numerous fundamental cellular functions.
548

Acknowledgments

We thank Dominic Fillion for assistance with microscopy, Denis Flaubert and the IRCM Proteomics Core for proteomics analysis, Gu Hua for HA-Ubiquitin plasmid, Sylvie Lahaie, Louis-Philippe Croteau and Farin B. Bourojeni for discussions, and Meirong Liang for technical support. This work was supported by project grants from the Canadian Institutes of Health Research (PJT-162225, MOP-77556, PJT-153053, and PJT-159839) to AK and a grant from the National Institutes of Health (R01 NS072129) to BG. CC received IRCM Jacques-Gauthier Scholarship. S. L. B. is a Fonds de recherche du Québec – Santé (FRQS) scholar. SSP is funded by IRCM Jean-Coutu Scholarship.

Author contribution

All authors: Conceptualisation, Writing – Editing and Review.

CC: Methodology, Investigation, Data Curation, Writing – Original Draft, Visualisation.

SLB: Methodology, Investigation, Data Curation, Visualisation, Supervision, Writing – Original Draft.

SSP: Methodology, Investigation, Data Curation, Visualisation.

XZ: Methodology, Investigation.

DCW: Methodology, Investigation.

MD: Methodology, Investigation, Resources, Data Curation, Visualisation, Supervision, Writing – Original Draft.

BG: Supervision, Funding Acquisition, Writing – Original Draft.

AK: Writing – Original Draft, Supervision, Project Administration, Supervision, Funding Acquisition.

Conflict of interest

The authors declare no competing financial interests.

578 **Materials and Methods**
579
580 **Vertebrate animals**
581 All animal experiments were carried out in accordance with the Canadian Council on Animal
582 Care guidelines and approved by the IRCM Animal Care Committee. Fertilized chicken eggs
583 (FERME GMS, Saint-Liboire, QC, Canada) were incubated at 38-39°C and staged according to
584 Hamburger and Hamilton (HH) (Hamburger and Hamilton, 1951). C57BL/6 mice were used for
585 hippocampal neuron collapse assay. Timed mating vaginal plug was designated as E0.5.
586
587 **Cell culture**
588 HeLa and HEK293T cells were maintained in DMEM (Thermo Fisher Scientific, #11965092)
589 supplemented with 10% Fetal Bovine Serum (FBS; Wisent Bioproducts, #080-150) and 1%
590 Penicillin/Streptomycin (Wisent Bioproducts, #450-200-EL) at 37°C with 5% CO_2. Tetracycline
591 inducible HeLa EPHB2-FLAG cells were generated by transfecting Flp-In T-REx HeLa cells with
592 EPHB2-BirA*-FLAG expression plasmid using Lipofectamine 3000 (Invitrogen, #L3000015)
593 followed by hygromycin selection (200µg/ml). Stable $CTRL^{CTRISPR}$ or $MYCBP2^{CRISPR}$ HeLa
594 EPHB2-FLAG cell lines were generated by infecting cells with packaged lentivirus, followed by
595 puromycin selection (1µg/ml). Lentivirus particles were packaged using MYCBP2 sgRNA
596 CRISPR plasmid designed to target the *MYCBP2* exon6 (pLentiCRISPR2-sgMYCBP2) and
597 pLentiCRISPR empty vector was used as Ctrl CRISPR. EPHB2-FLAG overexpression was
598 induced using 1µg/ml tetracycline simultaneously with cell starvation in DMEM supplemented
599 with 0.5%FBS, 1% penicillin/streptomycin for 12-20h. Prior to cell stimulation, Fc control
600 (Millipore, #401104), ephrinB1-Fc (R&D, #473-EB) or ephrinB2-Fc (R&D, #496-EB) were pre-
601 clustered using goat anti-human Fc IgG (Sigma, #I2136) in 4:1 ratio for 30min.
602
603 **Affinity purification - mass spectrometry**
604 HeLa EPHB2-FLAG cells cultured in DMEM supplemented with 0.5% FBS and 1µg/ml
605 tetracycline in 15cm cell culture plates for 20h, were treated with pre-clustered Fc control or
606 ephrinB2-Fc for 15min. After treatment, cells were washed twice with PBS and lysed using a
607 lysis buffer (50mM Tris, pH7.4; 150mM NaCl; 1% NP-40) supplemented with protease (Roche,
608 #11836153001) and phosphatase inhibitors (Roche, #04906837001). The lysates were collected
609 in 1.5ml Eppendorf tubes and centrifuged at 13,000rpm for 15min at 4°C. Supernatants were
610 transferred to new tubes with prewashed anti-FLAG agarose beads (Sigma, #A2220) and
611 incubated on a rotator overnight at 4°C. The following day, beads were washed four times using
612 50mM Ammonium Bicarbonate. The on-bead proteins were diluted in 2M Urea/50mM
613 ammonium bicarbonate and on-bead trypsin digestion was performed overnight at 37°C. The
614 samples were then reduced with 13 mM dithiothreitol at 37°C and, after cooling for 10min,
615 alkylated with 23 mM iodoacetamide at room temperature for 20min in the dark. The
616 supernatants were acidified with trifluoroacetic acid and cleaned from residual detergents and
617 reagents with MCX cartridges (Waters Oasis MCX 96-well Elution Plate) following the

618 manufacturer's instructions. After elution in 10% ammonium hydroxide /90% methanol (v/v),
619 samples were dried with a Speed-vac, reconstituted under agitation for 15min in 12µL of
620 2%ACN-1%FA and loaded into a 75µm i.d. × 150 mm Self-Pack C18 column installed in the
621 Easy-nLC II system (Proxeon Biosystems). Peptides were eluted with a two-slope gradient at a
622 flowrate of 250nL/min. Solvent B first increased from 2 to 35% in 100min and then from 35 to
623 80% B in 10min. The HPLC system was coupled to Orbitrap Fusion mass spectrometer (Thermo
624 Scientific) through a Nanospray Flex Ion Source. Nanospray and S-lens voltages were set to
625 1.3-1.7 kV and 60 V, respectively. Capillary temperature was set to 225°C. Full scan MS survey
626 spectra (m/z 360-1560) in profile mode were acquired in the Orbitrap with a resolution of 120,000
627 with a target value at 3e5. The 25 most intense peptide ions were fragmented in the HCD
628 collision cell and analyzed in the linear ion trap with a target value at 2e4 and a normalized
629 collision energy at 29 V. Target ions selected for fragmentation were dynamically excluded for
630 15 sec after two MS2 events.
631
632 **Mass spectrometry data analysis**
633 The peak list files were generated with Proteome Discoverer (version 2.3) using the following
634 parameters: minimum mass set to 500 Da, maximum mass set to 6000 Da, no grouping of
635 MS/MS spectra, precursor charge set to auto, and minimum number of fragment ions set to 5.
636 Protein database searching was performed with Mascot 2.6 (Matrix Science) against the UniProt
637 Human protein database. The mass tolerances for precursor and fragment ions were set to 10
638 ppm and 0.6 Da, respectively. Trypsin was used as the enzyme allowing for up to 1 missed
639 cleavage. Cysteine carbamidomethylation was specified as a fixed modification, and methionine
640 oxidation as variable modification. Data interpretation was performed using Scaffold (version 4.8)
641 and further statistical analysis was performed through ProHits integrated with SAINT
642 (Significance Analysis of INTeractome) (Liu et al., 2010).
643
644 **Cell lysis, co-immunoprecipitation and Western blotting**
645 Cells were washed with PBS, lysed with RIPA buffer (50mM Tris, pH 7.4; 150mM NaCl; 1% NP-
646 40; 0.1% SDS) supplemented with protease and phosphatase inhibitors. For co-IP experiments,
647 cells were lysed with co-IP buffer (50mM Tris, pH 7.4; 150mM NaCl; 0.1% NP-40) with protease
648 and phosphatase inhibitors. Cell lysates were centrifuged at 13,000 rpm for 20min at 4°C, then
649 the supernatants were collected, and total protein concentrations were quantified using BCA kit
650 (Thermo Scientific, #23225). For FLAG co-IP, 500-1000µg of total protein was incubated with
651 20-40 µl of prewashed anti-FLAG agarose beads (Sigma, #A2220) for 3h at 4°C. After incubation,
652 the beads were centrifuged at 2,600rpm for 1min at 4℃ and washed three times with the co-IP
653 buffer. The beads were resuspended in 2xSDS-PAGE loading buffer (5x loading buffer: Tris,
654 150mM, pH 6.8; SDS, 10%; Glyercol, 30%; b-Mercaptoethanol, 5%; Bromophenol Blue, 0.02%).
655 For western blotting, proteins were separated on 6-10% SDS-PAGE gels and transferred to
656 methanol pre-activated PVDF membranes (Millipore, #IPVH00010). For MYCBP2 blots, gels
657 were wet transferred overnight at 4°C using 33V. Membranes were incubated in blocking buffer

658 (TBST: 20mM Tris, pH 7.6; 150mM NaCl; 0.1% Tween 20; 5% skim milk) for 1h at room
659 temperature, followed by primary antibody incubation (1-2h at room temperature or overnight at
660 4°C) and corresponding secondary antibody incubation (1h at room temperature). Primary
661 antibodies were: rabbit polyclonal anti-MYCBP2 (Abcam, #ab86078; RRID:AB_1925230), rabbit
662 anti-pERK1/2 (Thr202/Tyr204; Cell Signaling Technology, #9101; RRID:AB_331646), rabbit
663 anti-ERK1/2 (Cell Signaling Technology, #9102; RRID:AB_330744), goat polyclonal anti-EPHB2
664 (R&D Systems, #AF467; RRID:AB_355375), mouse monoclonal anti-Actin (Sigma-Aldrich,
665 #A5441; RRID:AB_476744), mouse monoclonal anti-pTyr (PY20; Santa Cruz Biotechnology,
666 #sc-508; RRID:AB_628122), mouse monoclonal anti-GAPDH (Santa Cruz Biotechnology, #sc-
667 47724; RRID:AB_627678), mouse monoclonal anti-FLAG-HRP (Sigma-Aldrich, #A8592;
668 RRID:AB_439702), rabbit monoclonal anti-HA (Cell Signaling Technology, #3724;
669 RRID:AB_1549585), mouse monoclonal anti-MYC (Santa Cruz Biotechnology, #sc-40;
670 RRID:AB_627268), rabbit polyclonal anti-GFP (Thermo Fisher Scientific, #A-11122;
671 RRID:AB_221569). Secondary antibodies were: Donkey anti-Goat HRP (Jackson, 705-035-003),
672 Donkey anti-Mouse HRP (Jackson, 715-035-151), Donkey anti-Rabbit HRP (Jackson, 711-035-
673 152). After three washes with TBST, membranes were incubated with ECL reagent (Cytiva,
674 RPN2106) for 1min and chemiluminescence signal was acquired using film or Bio-Rad
675 ChemiDoc Imaging machine. Band intensity was quantified using ImageJ or Bio-Rad Image Lab
676 software.
677
678 **HeLa cell collapse assay**
679 HeLa-EPHB2 CTRL^{CRISPR} and MYCBP2^{CRISPR} cells were seeded on glass coverslips (Electron
680 Microscopy Sciences, #7223101) in 24 well plates at a density of 20 000 cells/well. After 24
681 hours, cell media was changed for DMEM supplemented with 0.5% FBS, 1% P/S and 1µg/ml
682 tetracycline to starve the cells and induce EPHB2 expression for 16-20 hours. Cells were then
683 stimulated with 1.5µg/ml of pre-clustered Fc control or ephrin-B2-Fc for 15min. Cells were fixed
684 with 3.2% paraformaldehyde (PFA), 6% sucrose in PBS for 12-15min. Nuclei were stained with
685 DAPI and F-actin with Phalloidin Alexa Fluor 568 conjugate (Thermo Fisher, #A12380). Images
686 were acquired using Zeiss LSM710 confocal microscope and 20x objective. Fully rounded cells
687 are scored as collapsed cells.
688
689 For time lapse imaging experiments, CTRL^{CRISPR} or *MYCBP2*^{CRISPR} cells were plated on
690 Poly-D-Lysine coated glass bottom 35mm dishes (MATTEK, #P35GC-1.5-10-C) at a density of
691 300,000 cells/dish. The next day, cells were transfected with 1.5µg of EPHB2-GFP plasmid for
692 4-5 h, using lipofectamine 3000 in opti-MEM (ThermoFisher, #31985070), and then media was
693 changed for DMEM supplemented with 0.5% FBS. The following day, the images were acquired
694 under Zeiss Spinning Disk Microscope using a 20x objective. During the imaging, the cells were
695 maintained at 37°C with 5% CO_2. Pre-clustered ephrinB2-Fc was added to a final concentration
696 of 2µg/mL directly into the dishes at the beginning of each experiment. The images were
697 acquired every minute for 1h.

698

699 **HeLa cell stripe assay**

700 Alternative ephrin-B2-Fc or Fc stripes were prepared using silicon matrices with a micro-well
701 system (Poliak et al., 2015). HeLa EPHB2 CTRL^{CRISPR} and MYCBP2^{CRISPR} cells, or HeLa EPHB2
702 cells transiently transfected with GFP-FBD1 wild-type or GFP-FBD1 mutant (GRR/AAA: G2404A,
703 R2406A, R2408A), were cultured with tetracycline for 20h, trypsinized and plated on stripes (~10
704 000 cells per carpet); see (Desbois et al., 2018) for specific sequences. The next day, cells were
705 fixed with paraformaldehyde (3.2% PFA, 6% sucrose in PBS), and stained with DAPI and
706 Phalloidin Alexa Fluor 488; or DAPI, Rabbit anti-GFP (Thermo Fisher Scientific, # A-11122;
707 RRID:AB_221569) and Phalloidin Alexa Fluor 647 (Abcam, #ab176759). Images were acquired
708 using Zeiss LSM710 confocal microscope and 20x objective (three vision fields for each carpet).
709 Cells on or off the ephrin-B2 stripes were decided by the nuclei localization of the cells.

710

711 **Ubiquitination assay**

712 HeLa EphB2 CTRL^{CRISPR} and MYCBP2^{CRISPR} cells were seeded in 6-well plates at a density of
713 0.5 million cells per well. Next day, cells were transfected with 1.2µg HA-Ubiquitin (gift of Gu
714 Hua) using lipofectamine 3000 (2µl/well) for 4-5h in opti-MEM (ThermoFisher, #31985070), then
715 media was changed to DMEM with 10%FBS. The following day, EPHB2 expression was induced
716 using 1µg/ml tetracycline in DMEM with 0.5% FBS for 12h followed by 2µg/ml Fc or eB2-Fc
717 treatment for 30min. After IP using anti-FLAG beads, precipitates were eluted with 2xSDS
718 loading buffer, resolved using 8% SDS gel and transferred onto PVDF membranes. Membranes
719 were blocked in 5% milk following an incubation with anti-HA antibody (Cell Signaling
720 Technology, #3724) to detect EPHB2 ubiquitination levels. The membrane was then stripped
721 using mild stripping buffer (1L: 15g glycine, 1g SDS, 10mL Tween 20, pH 2.2) and probed with
722 anti-FLAG antibody to reveal EPHB2 levels.

723

724 **Lysosome and proteasome inhibition**

725 HeLa EPHB2 CTRL^{CRISPR} and MYCBP2^{CRISPR} cells were seed in 6-well plates at a density of 0.5
726 million cells per well. Next day, EPHB2 overexpression was induced using 1µg/ml tetracycline
727 in DMEM with 10% FBS for 16h, followed by 26S proteasome inhibitor (MG132, 50 µM, Sigma,
728 #474790) or lysosome inhibitor treatment (BafilomycinA1, 0.2 µM, Sigma, #B1793; Chloroquine,
729 50 µM, Tocris, #4109) for 6hr.

730

731 **Chick *in ovo* electroporation**

732 Fertilized eggs (FERME GMS, Saint-Liboire, QC) were incubated in an incubator (Lyon
733 Technologies, model PRFWD) at 39°C with a humidity level of around 40%-60% according to
734 standard protocols. At HH stage.15-17, chick embryo spinal neural tubes were electroporated
735 with expression constructs (TSS20 Ovodyne electroporator at 30V, 5 pulses, 50ms wide,
736 1000ms interval). Following electroporation, eggs were sealed with double layer of parafilm
737 (Pechiney Plastic Packaging Company) and incubated till HH stage 24-26.

738
739 **Chick spinal explants stripe assay**
740 Alternative eprhinB2-Fc/Fc stripes were prepared using silicon matrices with a micro-well system
741 and pre-coated with laminin. At HH stage 24-26, chick embryos were harvested, and the lumbar
742 part neural tubes were dissected with tungsten needles (World Precision Instruments) in MN
743 medium (20ml motor neuron medium: 19.2ml Neurobasal medium, 400µl B27 supplement, 200µl
744 50mM L-glutamic acid, 200µl 100xP/S antibiotics,73mg L-glutamine). The lumbar neural tube
745 was then cut into around 20 explants and the explants were plated on stripes (a 1cmx1cm square
746 covers the whole stripe area). After overnight incubation, the explants were fixed with 4% PFA
747 for 12min at 37°C, washed once with PBS, and incubated with blocking buffer, primary antibodies,
748 and secondary antibodies. After three times PBS washes, the explants on stripes were mounted
749 and explants with extensions were imaged using LSM710 (at least three explants per carpet).
750 The percentage of branches on ephrinB2 stripes was calculated using the total length of
751 branches localized on ephrinB2 stripes divided by the total length of the branches of the explant.
752
753 **Dissociated mouse hippocampal neuron culture and electroporation**
754 Primary hippocampal neurons were cultured from wild-type C57BL/6 mice at embryonic day 16–
755 18 (E16-18). The hippocampi were dissected out and collected in 4.5ml dissection buffer
756 (calcium- and magnesium-free Hank's BSS: 500 ml distilled water (Gibco, #15230162), 56.8 ml
757 10xHBSS (Gibco, #14185052), 5.68ml 1M HEPES (Gibco, #15630080), 2.84ml HyClone
758 (Thermo Scientific, #SV30010)). Hippocampi were added with 0.5ml 2.5%Tyrpsin and incubated
759 at 37°C for 13-15min. After 5 times of thorough wash with dissection buffer, hippocampal
760 neurons were dissociated in 0.8ml DMEM (Gibco, #11965118) with 10% FBS (Wisent
761 Bioproducts, 080-150) by pipetting 10 times up and down. Then cell numbers were counted and
762 desired number of neurons were directed for electroporation. After spin down at 2,000 rpm for
763 2min, dissociated hippocampal neurons ($1x10^6$/condition) were resuspended with 100µl
764 homemade nucleofection solution, mixed with 5ug of DNA, and transferred into the aluminum
765 cuvettes (AMAXA/Lonza). Electroporation was achieved by Nucleofector I (AMAXA/Lonza)
766 using program O-05 (Mouse CNS neurons). 1ml Plating Medium (PM; 500ml MEM (Sigma,
767 #M4655), 17.5ml 20% Glucose (Sigma, #G8270), 5.8ml 100mM pyruvate (Sigma, #P2256),
768 58ml heat-inactivated horse serum (Thermo Scientific, #26050088)) was added to the cuvettes
769 immediately, and desired number of neurons were plated on 1mg/ml Poly-L-Lysine (Sigma,
770 #P2636) coated coverslips in 12-well plate. At 1 day *in vitro* (DIV1), medium was replaced with
771 Neuron growth and maintenance medium (NBG; 500ml Neurobasal medium (Gibco,
772 #21103049), 10ml SM1 neuronal supplement (Stemcell, #05711), and 1.25ml GlutaMAX-I
773 (Gibco, #35050)).
774
775 **Hippocampal neuron growth cone collapse assay**
776 Electroporated hippocampal neurons were cultured on glass coverslips (18 mm, 100 thousand
777 neurons/well in a 12-well plate). At DIV2, the neurons were treated with pre-clustered ephrinB1-

Fc, ephrinB2-Fc or Fc control in NBG medium at a final concentration of 2μg/ml for 60min at 37°C. After treatment, neurons were fixed with paraformaldehyde (3.2% PFA,6% sucrose in PBS) for 12min, followed by two PBS washes, and blocked with Blocking Buffer (PBS, 0.15% TritonX-100, 2% FBS) for 60min at room temperature. Neurons were then incubated with rabbit anti-GFP antibody (1:5000, Thermo Fisher Scientific, #A11122; RRID:AB_221569) in Blocking Buffer for 90min at room temperature. Followed by three PBS washes, neurons were incubated with DAPI, donkey anti-rabbit IgG Alexa Fluor 488 conjugate (1:1000, Jacksonimmuno, #711545152) and Phalloidin Alexa Fluor 568 conjugate (1:300, Invitrogen, #A12380) in Blocking Buffer for 60min. Neurons on coverslips were then washed and mounted on microscope slides (Fisherbrand, #1255015). Collapsed growth cones were scored using followed criteria.

Collapsed hippocampal neuron growth cone quantification

Neuron selection: only neurons with moderate GFP staining (neurons with strong GFP signalling were excluded) and only neurons with more than three branches were scored. Branch selection: branches shorter than the diameter of the neuron cell body were excluded; branches intermingling with others were excluded. Collapsed growth cone: growth cones of a fan shape are scored as full, growth cones with a width smaller than that of the branches are scored as collapsed, and growth cones' size in between are scored as "hard to tell". The collapse rate was calculated using collapse growth cone numbers divided by the total growth cone numbers.

Microscopy and imaging

HeLa cell collapse assay images were acquired using Leica DM6 or Zeiss LSM710 confocal microscopy. Stripe assay and growth cone collapse assay images were acquired with a Zeiss LSM710 or LSM700 confocal microscope.

Quantification and statistical analysis

All cell counts, collapsed/uncollapsed visualization and explant neurite length measurements were performed with ImageJ 2.9.0 (Schindelin et al., 2012). All numbers are illustrated in figure legends. In western blotting, each n represents one independent experiment; in neuron growth cone collapse assay, each n represents one independent experiment with neurons pooled from multiple embryos. All data statistical analyses were performed using GraphPad Prism 9.1.1. Test methods and p values were described in figure legends, with p value 0.05 as a significance threshold.

Data Availability

The mass spectrometry proteomics data have been deposited to the ProteomeXchange Consortium via the PRIDE partner repository (Perez-Riverol et al., 2019) with the dataset identifier PXD041786 and 10.6019/PXD041786.

817 ***C. elegans* genetics and strains**

818 *C. elegans* N2 isolate was used for all experiments. Animals were maintained using standard
819 procedures. The following mutant alleles were used: *vab-1*(*dx31*) II, *fsn-1*(*gk429*) III, *rpm-1*(*ju44*)
820 V, *glo-4*(*ok623*) V. The integrated transgene used to evaluate axon termination was *muIs32*
821 [$P_{mec\text{-}7}$GFP] II. For genetic analysis the animals were grown at 23℃.

822

823 Transgenic extrachromosomal arrays were generated using standard microinjection
824 procedures for *C. elegans*. *vab-1* minigene (pCZ47) was injected at either 25 ng/µL or 50 ng/µL,
825 and co-injection markers used for transgene selection were either neomycin resistance (pBG-
826 264) or P*ttx-3*::RFP (pBG-41). pBluescript (pBG-49) was used to reach a final concentration of
827 100 ng/µl in all injection mixes. pCZ47 was a gift from Andrew Chisholm (Addgene plasmid #
828 128414 ; RRID:Addgene_128414)

829

830 ***C. elegans* axon termination analysis and imaging**

831 Axon termination defects were defined as PLM axons that extended beyond the normal
832 termination point adjacent to the ALM cell body. Two different failed termination phenotypes
833 were scored: axon overextension (moderate phenotype) where the PLM axon grew beyond ALM
834 cell body, axons that overextend and form a ventral hook (severe phenotype). To quantify axon
835 termination defects, 20-30 young adult animals were anesthetized (10 µM levamisole in M9
836 buffer) on a 2% agar pad on glass slides and visualized with a Leica DM5000 B (CTR5000)
837 epifluorescent microscope (40x oil-immersion objective). For image acquisition, young adult
838 animals were mounted on a 3% agarose pad and a Zeiss LSM 710 (40x oil-immersion objective)
839 was used to generate z stacks.

840

841 For statistical analysis of axon termination defects, comparisons were done using a
842 Student's *t*-test with Bonferroni correction on GraphPad Prism software. Error bars represent
843 standard error of the mean (SEM). Significance was defined as $p < 0.05$ after Bonferroni
844 correction. Bar graphs represent averages from 8 to 10 counts (20–30 animals/count) obtained
845 from eight or more independent experiments for each genotype. For transgenic rescue
846 experiments, data shown in Figure 8B was obtained from two, independently derived transgenic
847 extrachromosomal arrays.

848

849

850 **Figures and figure legends**

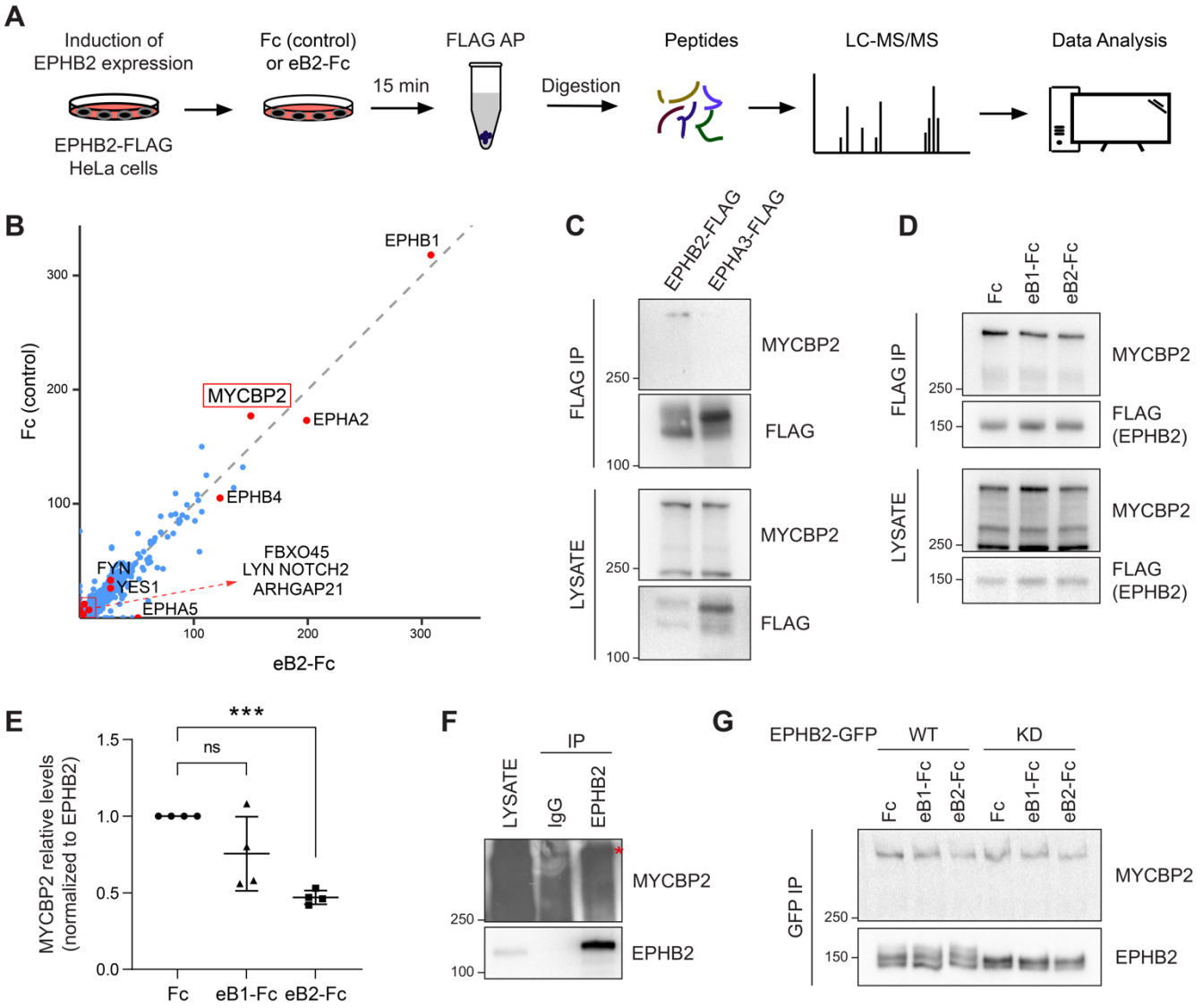

851

852 **Figure 1. MS-proteomics and biochemistry in HeLa cells identifies MYCBP2 as EPHB2 binding**
853 **protein.**
854 A) Schematic of EPHB2 affinity purification coupled to mass spectrometry (AP-MS) workflow. B) Scatter
855 plot of AP-MS data showing known and putative EPHB2 binding proteins, including MYCBP2. Y axis and
856 X axes represent the average spectral counts of the identified protein hits in the EPHB2 protein
857 complexes from cells stimulated with Fc control or ephrin-B2 (eB2-Fc), respectively. C) In HEK 293T cells,
858 endogenous MYCBP2 is pulled down by transiently overexpressed EPHB2-FLAG but not by EPHA3-
859 FLAG. D) In EPHB2-FLAG stable HeLa cell line, ephrin-B stimulation reduces the interaction between
860 MYCBP2 and EPHB2. E) Quantification of MYCBP2-EPHB2 association intensity after Fc, ephrin-B1
861 (eB2-Fc) or ephrin-B2 (eB2-Fc) treatment (eB1-Fc, p=0.1365; eB2-Fc, p=0.0002; one-sample t-test).
862 Error bars represent standard deviation (SD). F) Representative image of MYCBP2 pull down with anti-
863 EPHB2 or IgG control antibodies from whole rat cerebral tissue lysates. Asterisk indicates MYCBP2. G)

Representative images from western blot analysis of endogenous MYCBP2 following IP of GFP-EPHB2 wild-type (WT) or its kinase dead (KD) counterpart.

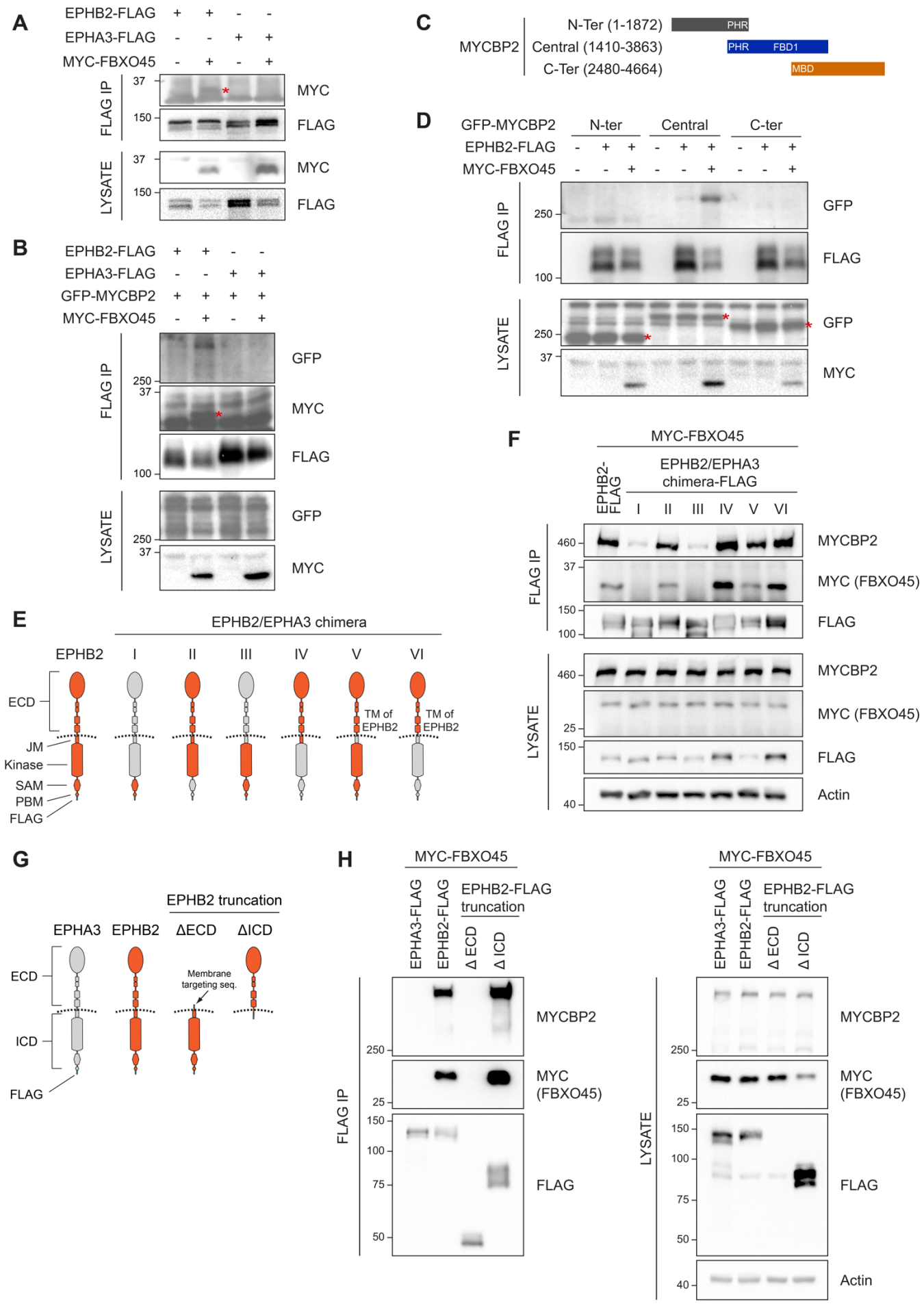
A
EPHB2-FLAG + + - -
EPHA3-FLAG - - + +
MYC-FBXO45 - + - +
FLAG IP
LYSATE
37
150
MYC
FLAG
B
EPHB2-FLAG + + - -
EPHA3-FLAG - - + +
GFP-MYCBP2 + + + +
MYC-FBXO45 - + - +
FLAG IP
LYSATE
250
37
100
GFP
MYC
FLAG
C
MYCBP2
N-Ter (1-1872)
Central (1410-3863)
C-Ter (2480-4664)
PHR
FBD1
MBD
D
GFP-MYCBP2
N-ter
Central
C-ter
EPHB2-FLAG
MYC-FBXO45
FLAG IP
LYSATE
250
100
37
GFP
FLAG
MYC
E
EPHB2/EPHA3 chimera
EPHB2
I
II
III
IV
V
VI
ECD
JM
Kinase
SAM
PBM
FLAG
TM of EPHB2
F
MYC-FBXO45
EPHB2-FLAG
EPHB2/EPHA3 chimera-FLAG
FLAG IP
LYSATE
460
37
150
100
25
40
MYCBP2
MYC (FBXO45)
FLAG
Actin
G
EPHB2 truncation
EPHA3
EPHB2
ΔECD
ΔICD
ECD
ICD
FLAG
Membrane targeting seq.
H
MYC-FBXO45
EPHA3-FLAG
EPHB2-FLAG
EPHB2-FLAG truncation
Δ ECD
Δ ICD
FLAG IP
LYSATE
250
25
150
100
75
50
40
MYCBP2
MYC (FBXO45)
FLAG
Actin

868 **Figure 2. Mapping binding regions for EPHB2-MYCBP2 reveals role of FBXO45 in this interaction.**
869 A) Co-IP of EPHB2-FLAG with MYC-FBXO45 using transfected HEK293 cells. EPHB2 co-precipitates
870 FBXO45, but EPHA3 does not. Asterisk indicates MYC-FBXO45. B) In HEK 293T cells, FBXO45
871 overexpression enhances EPHB2-MYCBP2 binding. Asterisk indicates MYC-FBXO45. C) Schematic
872 representation of MYCBP2 N-terminal, Central and C-terminal fragments. D) Co-IP of EPHB2-FLAG with
873 GFP-MYCBP2 fragments in HEK 293T cells. EPHB2 coprecipitates with MYCBP2 central fragment.
874 Asterisks indicate GFP-MYCBP2 fragments. E) Schematic of chimeric domain swapping of EPHB2
875 (orange) and EPHA3 (grey). F) Co-IP of MYC-FBXO45 and endogenous MYCBP2 with EPHB2/EPHA3
876 domain swapped chimeras. G) Schematic representation of EPHB2 ΔECD (extracellular domain) and
877 ΔICD (intracellular domain) truncations. H) Co-IP of endogenous MYCBP2 with EPHA3, EPHB2 and
878 EPHB2 truncation mutants. ECD, extracellular domain; TM, transmembrane; JM, juxtamembrane; SAM,
879 Sterile alpha motif; PBM, PDZ (PSD-95, Dlg1, Zo-1) binding motif.
880

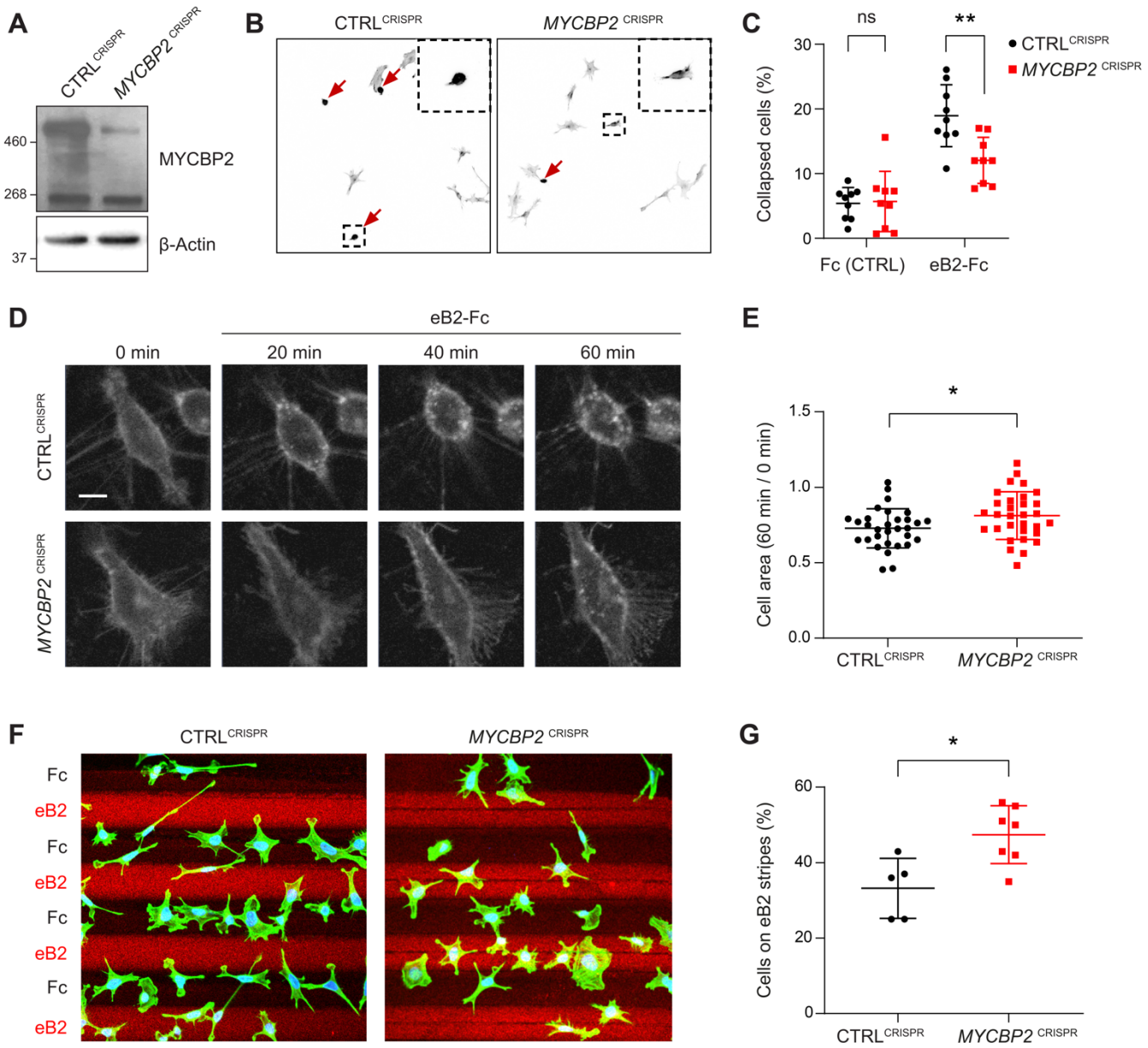

Figure 3. MYCBP2 CRISPR HeLa cells exhibit reduced ephrin-B2 evoked cell retraction and ephrin-B2 stripe avoidance.

A) MYCBP2 is reduced in HeLa *MYCBP2*^{CRISPR} cells generated by sgRNA targeting MYCBP2 exon 6. B) Representative images of cell collapse assays using CTRL^{CRISPR} or *MYCBP2*^{CRISPR} HeLa cells that were stimulated with ephrin-B2. Red arrows indicate rounded/collapsed cells. C) Quantification of collapsed cells. Statistical significance between CTRL^{CRISPR} and *MYCBP2*^{CRISPR} cells was determined using two-way ANOVA followed by Sidak's multiple comparison test (Fc, p=0.9841; eB2-Fc, p=0.0017). D) Representative time-lapse sequences of CTRL^{CRISPR} and *MYCBP2*^{CRISPR} HeLa cells after ephrin-B2 treatment. E) Quantification of cell area reduction after 60 min exposure to ephrin-B2 (p=0.0268, two-tailed unpaired t test). F) Ephrin-B2 stripe assays using CTRL^{CRISPR} or *MYCBP2*^{CRISPR} HeLa cells. Cells are visualized with Phalloidin 488 staining and nuclei are stained with DAPI (black, Fc stripes; red, ephrin-

893 B2 stripes). G) Quantification of cells present on ephrin-B2 stripes (%). Statistical significance was
894 determined using two-tailed unpaired t-test (p=0.0109). Error bars represent SD.
895

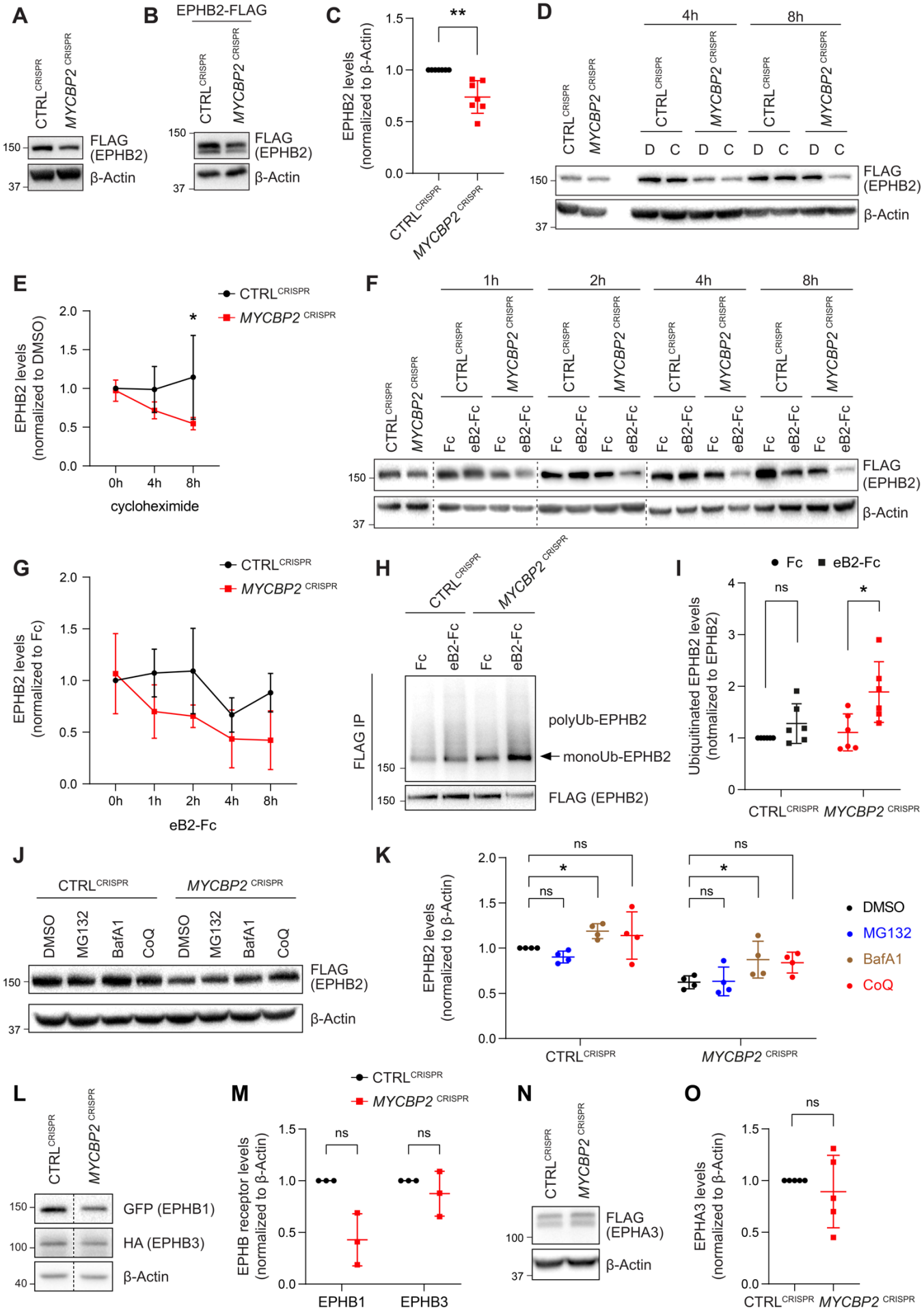
A
CTRL CRISPR
MYCBP2 CRISPR
150
FLAG (EPHB2)
β-Actin
37
B
EPHB2-FLAG
CTRL CRISPR
MYCBP2 CRISPR
150
FLAG (EPHB2)
β-Actin
37
C
EPHB2 levels (normalized to β-Actin)
**
1.5
1.0
0.5
0.0
CTRL CRISPR
MYCBP2 CRISPR
D
4h
8h
CTRL CRISPR
MYCBP2 CRISPR
D C D C D C D C
150
FLAG (EPHB2)
β-Actin
37
E
CTRL CRISPR
MYCBP2 CRISPR
EPHB2 levels (normalized to DMSO)
*
2.0
1.5
1.0
0.5
0.0
0h 4h 8h
cycloheximide
F
1h
2h
4h
8h
CTRL CRISPR
MYCBP2 CRISPR
Fc eB2-Fc
150
FLAG (EPHB2)
β-Actin
37
G
CTRL CRISPR
MYCBP2 CRISPR
EPHB2 levels (normalized to Fc)
2.0
1.5
1.0
0.5
0.0
0h 1h 2h 4h 8h
eB2-Fc
H
CTRL CRISPR
MYCBP2 CRISPR
Fc eB2-Fc Fc eB2-Fc
FLAG IP
polyUb-EPHB2
monoUb-EPHB2
150
FLAG (EPHB2)
150
I
Fc eB2-Fc
Ubiquitinated EPHB2 levels (notmalized to EPHB2)
ns
*
4
3
2
1
0
CTRL CRISPR
MYCBP2 CRISPR
J
CTRL CRISPR
MYCBP2 CRISPR
DMSO MG132 BafA1 CoQ DMSO MG132 BafA1 CoQ
150
FLAG (EPHB2)
β-Actin
37
K
EPHB2 levels (normalized to β-Actin)
ns
*
ns
ns
*
ns
2.0
1.5
1.0
0.5
0.0
CTRL CRISPR
MYCBP2 CRISPR
DMSO
MG132
BafA1
CoQ
L
CTRL CRISPR
MYCBP2 CRISPR
150
GFP (EPHB1)
100
HA (EPHB3)
β-Actin
40
M
CTRL CRISPR
MYCBP2 CRISPR
EPHB receptor levels (normalized to β-Actin)
ns
ns
1.5
1.0
0.5
0.0
EPHB1
EPHB3
N
CTRL CRISPR
MYCBP2 CRISPR
100
FLAG (EPHA3)
β-Actin
37
O
EPHA3 levels (normalized to β-Actin)
ns
1.5
1.0
0.5
0.0
CTRL CRISPR
MYCBP2 CRISPR

896

897 **Figure 4. MYCBP2 loss-of-function increases EPHB2 protein turnover in HeLa cells.**
898 A) Induced EPHB2-FLAG expression is reduced in *MYCBP2*^{CRISPR} HeLa cells. B) Western blotting for
899 transfected EPHB2-FLAG in CTRL^{CRISPR} and *MYCBP2*^{CRISPR} cells. C) Quantification of transfected
900 EPHB2-FLAG levels (p=0.0046, one-sample t-test). D) Representative western blot of EPHB2-FLAG in
901 CTRL^{CRISPR} and *MYCBP2*^{CRISPR} cells treated with DMSO or cycloheximide for 4h and 8h. E) Quantification
902 of EPHB2-FLAG turnover with cycloheximide (CTRL^{CRISPR} vs. *MYCBP2*^{CRISPR} at 8h eB2-Fc stimulation,
903 p= 0.0474, two-way ANOVA followed by Tukey's multiple comparison test). F) Western blot showing
904 EPHB2-FLAG degradation when cells are challenged with ephrin-B2 (1µg/ml) for different periods of time.
905 G) Quantification of ephrin-B2-evoked EPHB2 degradation (ns, not significant; two-way ANOVA followed
906 by Tukey's multiple comparison test). H) Western blot of EPHB2 ubiquitination in CTRL^{CRISPR} and
907 *MYCBP2*^{CRISPR} cells. I) Quantification of ubiquitinated EPHB2. CTRL^{CRISPR} cells stimulated with Fc vs.
908 eB2-Fc, p= 0.1349 (One sample t-test); *MYCBP2*^{CRISPR} cells stimulated with Fc vs. EB2-Fc, p= 0.0195
909 (Unpaired two-tailed t-test). J) After tetracycline induction of EPHB2-FLAG expression for 16hrs,
910 CTRL^{CRISPR} and *MYCBP2*^{CRISPR} HeLa cells were treated with DMSO (1:500) or inhibitors of the
911 proteasome (MG132 50µM) or lysosome (BafA1 0.2µM; CoQ 50µM) for 6 hours, and EPHB2 levels were
912 analysed by western blotting. K) Quantification of EPHB2 levels following treatment with proteasome or
913 lysosome inhibitors. Statistical significance for the comparison between CTRL^{CRISPR} cells treated with
914 DMSO or inhibitors was determined by one-sample t-test (MG132, p=0.0598; BafA1, p=0.0200; CoQ,
915 p=0.3632), whereas statistical significance for the comparison between *MYCBP2*^{CRISPR} cells treated with
916 DMSO and individual inhibitors was determined by two-tailed paired t-test (MG132, p=0.8893; BafA1,
917 p=0.0361; CoQ, p=0.0835). L) GFP-EPHB1 and HA-EPHB3 transfected into CTRL^{CRISPR} and
918 *MYCBP2*^{CRISPR} HeLa cells and detected by Western blot. M) Quantification of GFP-EPHB1 and HA-
919 EPHB3 levels (EPHB1, p=0.0588; EPHB3, p=0.4253; one-sample t-test). N) FLAG-EPHA3 transfected
920 into CTRL^{CRISPR} and *MYCBP2*^{CRISPR} HeLa cells and detected by WB. O) Quantification of FLAG-EPHA3
921 (p=0.5369, one-sample t-test). Error bars represent SD.
922

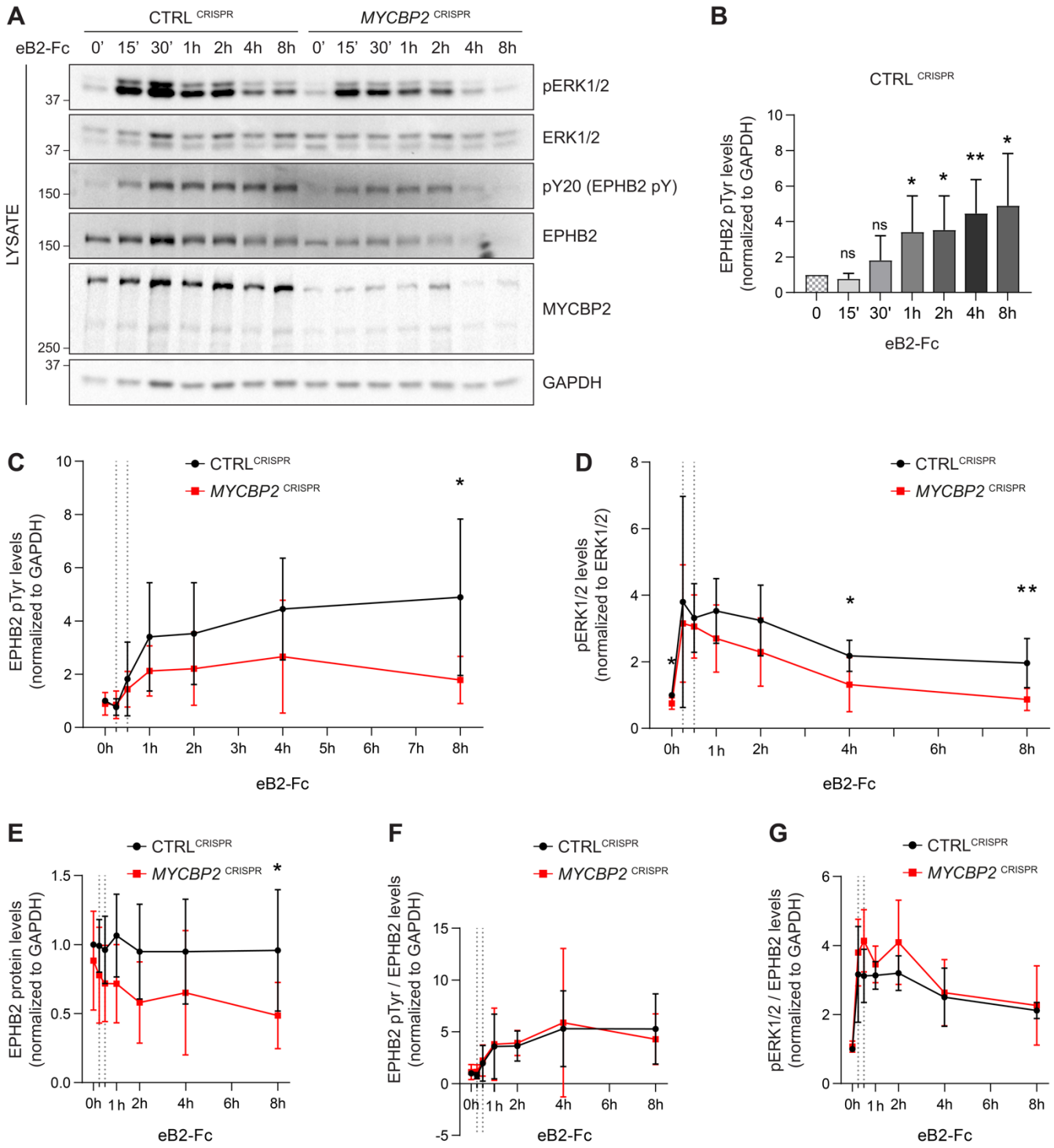

Figure 5. MYCBP2 depletion impairs EPHB2 phosphorylation and ERK1/2 activation in HeLa cells. A) Representative western blot for pERK1/2 and pTyr-EPHB2 detected in CTRL^{CRISPR} and *MYCBP2*^{CRISPR} cells treated with ephrin-B2 (eB2-Fc) for different periods (n=6). Membranes were striped and reblotted with anti-ERK1/2, anti-EPHB2, anti-GAPDH and anti-MYCBP2 antibodies as controls. B) Quantification of EPHB2 tyrosine phosphorylation in CTRL^{CRISPR} cells evoked by ephrin-B2 treatment (15 min, p=0.1363;

929 30 min, p=0.2056; 1h, p=0.0342; 2h, p=0.0234; 4h, p=0.0068; 8h, p= 0.0231; one-sample t-test). C)
930 Quantification of EPHB2 tyrosine phosphorylation in CTRL^{CRISPR} and *MYCBP2*^{CRISPR} HeLa cells
931 (unstimulated, p=0.5589, one-sample t-test; stimulated for 15 min, p=0.7463; 30 min, p=0.5520; 1h,
932 p=0.1920; 2h, p=0.2009; 4h, p=0.1550; 8h, p=0.0331; two-tailed unpaired t-test). D) Quantification of
933 pERK1/2 in CTRL^{CRISPR} and *MYCBP2*^{CRISPR} HeLa cells (0 min, p=0.0168, one-sample t-test; 15 min,
934 p=0.6695; 30 min, p= 0.6649; 1h, p= 0.1776; 2h, p= 0.1479; 4h, p= 0.0494; 8h, p= 0.0078; two-tailed
935 unpaired t-test). E) Quantification of EPHB2 in CTRL^{CRISPR} and *MYCBP2*^{CRISPR} HeLa (0 min, p=0.4604,
936 one-sample t-test; 15 min, p=0.2222; 30 min, p=0.1376; 1h, p=0.0651; 2h, p=0.0736; 4h, p=0.2451; 8h,
937 p=0.0437, two-tailed unpaired t-test). F) Quantification of ephrin-B2-evoked EPHB2 tyrosine
938 phosphorylation levels relative to total EPHB2 protein levels (0 min, p=0.7058, one-sample t-test; 15 min,
939 p=0.2464; 30 min, p=0.7835; 1h, p=0.9164; 2h, p=0.7196; 4h, p=0.8625; 8h, p=0.5750, two-tailed
940 unpaired t-test). G) Quantification of ephrin-B2-evoked pERK1/2 relative to EPHB2 total protein levels (0
941 min, p=0.3308, one-sample t-test; 15 min, p=0.3856; 30 min, p=0.0624; 1h, p=0.2683; 2h, p=0.1284; 4h,
942 p=0.7998; 8h, p=0.7790, two-tailed unpaired t-test. Error bars represent SD.
943

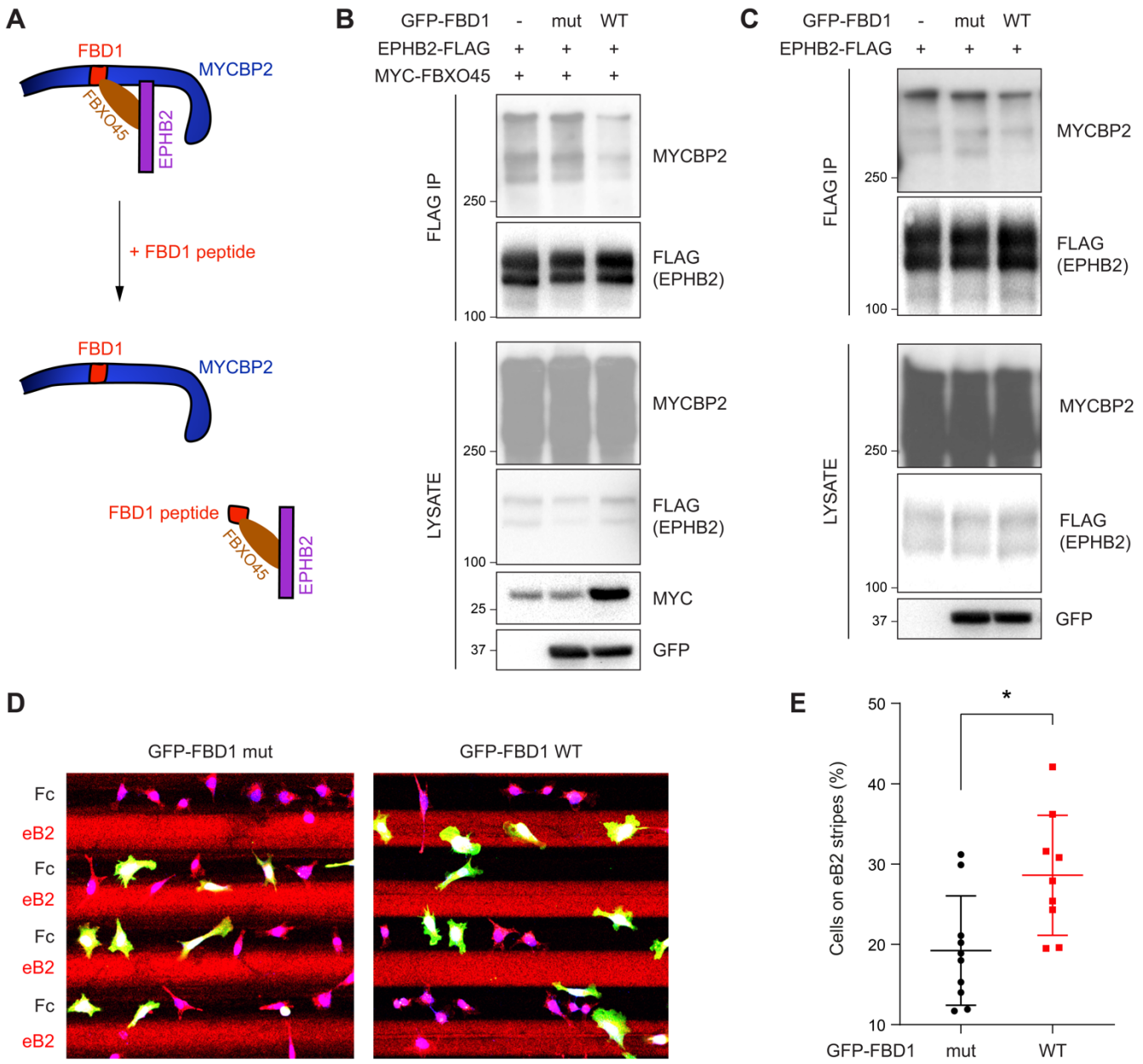

Figure 6. Exogenous FBD1 fragment of MYCBP2 disrupts EPHB2-MYCBP2 binding and impairs EPHB2 function in HeLa cells.

A) Schematic illustrating competition of exogenous MYCBP2-FBD1 fragment that disrupts MYCBP2-FBXO45 binding and leads to MYCBP2 reduction in EPHB2 complexes. B) Exogenous FBD1 WT overexpression leads to reduced EPHB2-MYCBP2 binding in HEK293 cells despite co-expression of FBXO45. C) FBD1 overexpression also disrupts EPHB2-MYCBP2 binding in the absence of FBXO45 overexpression. D) Representative images of ephrin-B2 stripe assays using HeLa cells expressing GFP-FBD1 mut or GFP-FBD1 WT. E) Quantification of cells present on eB2 stripes (p=0.0107, two-tailed unpaired t-test). Error bars represent SD.

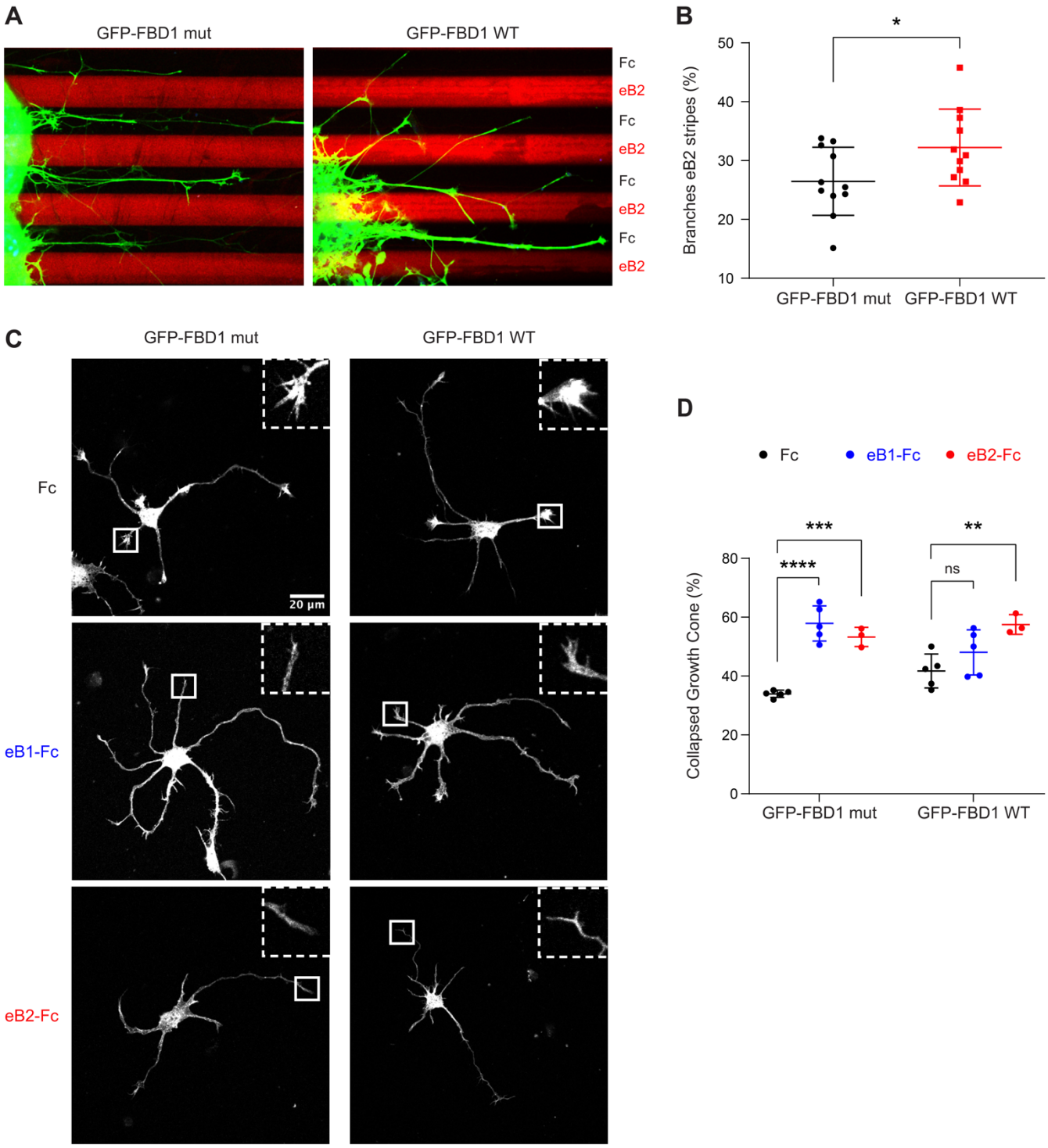

Figure 7. Exogenous FBD1 overexpression impairs EPH receptor functions in chick spinal cord explants and mouse hippocampal neurons.

A) Representative images of ephrin-B2 stripe assays with chick embryonic spinal cord explants overexpressing GFP-FBD1 mut (negative control) or GFP-FBD1 WT. B) Quantification of GFP-positive branches present on ephrin-B2 stripes (GFP-FBD1 mut vs. GFP-FBD1 WT, p=0.0410, two-tailed

960 unpaired t-test). C) Representative images of DIV2 mouse hippocampal neurons overexpressing GFP-
961 FBD1 mut or GFP-FBD1 WT and challenged with Fc control, ephrin-B1 (eB1-Fc) or ephrin-B2 (eB2-Fc).
962 D) Quantification of growth cone collapse rate for hippocampal neurites. GFP-FBD1 mut: Fc vs. eB1-Fc,
963 p=<0.0001; Fc vs. eB2-Fc, p=0.0008; GFP-FBD1 WT: Fc vs. eB1-Fc p=0.4357; Fc vs eB2-Fc p=0.0065.
964 Two-way ANOVA followed by Tukey's multiple comparisons test. Error bars represent SD.
965

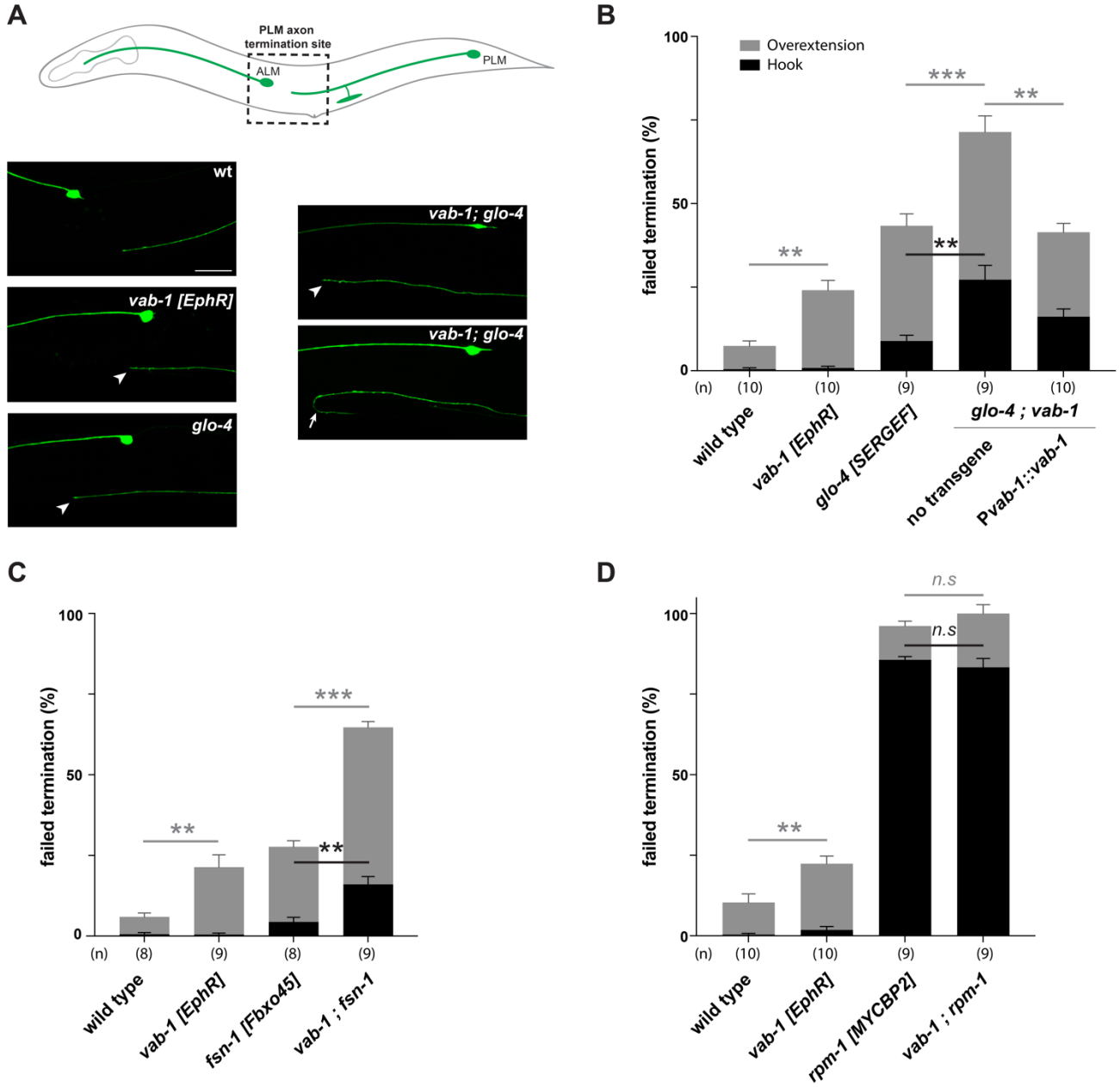

Figure 8*. Vab-1* ephrin receptor interacts genetically with *MYCBP2/rpm-1 in C. elegans*.

A) Schematic of axon morphology and axon termination site for PLM mechanosensory neurons. Shown are representative images of PLM axon termination observed for indicated genotypes. Moderate overextension defects (arrowhead) were observed in *vab-1* and *glo-4* single mutants. Both overextension defects (arrowhead) and more severe hook defects (arrow) were observed in *vab-1; glo-4* double mutants. B) Quantitation of axon termination defects for indicated genotypes. *vab-1; glo-4* double mutants show enhanced frequency of both severe hook (black) and moderate overextension (grey) axon termination defects. Overextension defects are significantly reduced by transgenic expression of VAB-1. C) Quantitation of axon termination defects for indicated genotypes. *vab-1; fsn-1* double mutants show enhanced termination defects. D) Quantitation of axon termination defect for indicated genotypes. Axon

977 termination defects are not enhanced nor suppressed in *vab-1; rpm-1* double mutants compared to *rpm-*
978 *1* single mutants. n is defined as a single count of 20-30 animals. Means are shown from 8 to 10 counts
979 (20-30 animals per count) for each genotype, and error bars represent SEM. Significance determined
980 using Student's *t*-test with Bonferroni correction. ** $p < 0.01$; *** $p < 0.001$; n.s, not significant. Scale bar
981 is 20 μm.
982
983
984

985 **References**

986

987 Al-Abdi, L., Desbois, M., Rusnac, D.V., Sulaiman, R.A., Rosenfeld, J.A., Lalani, S., Murdock, D.R., Burrage,
988 L.C., Undiagnosed Diseases, N., Billie Au, P.Y.*, et al.* (2022). Loss-of-function variants in MYCBP2 cause
989 neurobehavioural phenotypes and corpus callosum defects. Brain, awac364.

990 Babetto, E., Beirowski, B., Russler, E.V., Milbrandt, J., and Diantonio, A. (2013). The Phr1 ubiquitin ligase
991 promotes injury-induced axon self-destruction. Cell Reports *3*, 1422-1429.

992 Banerjee, S.L., Lessard, F., Chartier, F.J.M., Jacquet, K., Osornio-Hernandez, A.I., Teyssier, V., Ghani, K.,
993 Lavoie, N., Lavoie, J.N., Caruso, M.*, et al.* (2022). EPH receptor tyrosine kinases phosphorylate the PAR-3
994 scaffold protein to modulate downstream signaling networks. Cell Rep *40*, 111031.

995 Binns, K.L., Taylor, P.P., Sicheri, F., Pawson, T., and Holland, S.J. (2000). Phosphorylation of tyrosine
996 residues in the kinase domain and juxtamembrane region regulates the biological and catalytic activities
997 of Eph receptors. Mol Cell Biol *20*, 4791-4805.

998 Bloom, A.J., Miller, B.R., Sanes, J.R., and DiAntonio, A. (2007). The requirement for Phr1 in CNS axon tract
999 formation reveals the corticostriatal boundary as a choice point for cortical axons. Genes Dev *21*, 2593-
1000 2606.

1001 Borgen, M.A., Wang, D., and Grill, B. (2017). RPM-1 regulates axon termination by affecting growth cone
1002 collapse and microtubule stability. Development *144*, 4658-4672.

1003 Bush, J.O. (2022). Cellular and molecular mechanisms of EPH/EPHRIN signaling in evolution and
1004 development. Curr Top Dev Biol *149*, 153-201.

1005 Bush, J.O., and Soriano, P. (2010). Ephrin-B1 forward signaling regulates craniofacial morphogenesis by
1006 controlling cell proliferation across Eph-ephrin boundaries. Genes Dev *24*, 2068-2080.

1007 Cissé, M., Halabisky, B., Harris, J., Devidze, N., Dubal, D.B., Sun, B., Orr, A., Lotz, G., Kim, D.H., Hamto, P.*,*
1008 *et al.* (2011). Reversing EphB2 depletion rescues cognitive functions in Alzheimer model. Nature *469*, 47-
1009 52.

1010 Collins, C.A., Wairkar, Y.P., Johnson, S.L., and DiAntonio, A. (2006). Highwire restrains synaptic growth by
1011 attenuating a MAP kinase signal. Neuron *51*, 57-69.

1012 Crawley, O., Opperman, K.J., Desbois, M., Adrados, I., Borgen, M.A., Giles, A.C., Duckett, D.R., and Grill,
1013 B. (2019). Autophagy is inhibited by ubiquitin ligase activity in the nervous system. Nat Commun *10*, 5017.

1014 D'Souza, J., Hendricks, M., Le Guyader, S., Subburaju, S., Grunewald, B., Scholich, K., and Jesuthasan, S.
1015 (2005). Formation of the retinotectal projection requires Esrom, an ortholog of PAM (protein associated
1016 with Myc). Development *132*, 247-256.

1017 Dalva, M.B., Takasu, M.A., Lin, M.Z., Shamah, S.M., Hu, L., Gale, N.W., and Greenberg, M.E. (2000). EphB
1018 receptors interact with NMDA receptors and regulate excitatory synapse formation. Cell *103*, 945-956.

1019 Depaepe, V., Suarez-Gonzalez, N., Dufour, A., Passante, L., Gorski, J.A., Jones, K.R., Ledent, C., and
1020 Vanderhaeghen, P. (2005). Ephrin signalling controls brain size by regulating apoptosis of neural
1021 progenitors. Nature *435*, 1244-1250.

1022 Desbois, M., Crawley, O., Evans, P.R., Baker, S.T., Masuho, I., Yasuda, R., and Grill, B. (2018). PAM forms
1023 an atypical SCF ubiquitin ligase complex that ubiquitinates and degrades NMNAT2. J Biol Chem *293*,
1024 13897-13909.

1025 Desbois, M., Opperman, K.J., Amezquita, J., Gaglio, G., Crawley, O., and Grill, B. (2022). Ubiquitin ligase
1026 activity inhibits Cdk5 to control axon termination. PLoS Genet *18*, e1010152.

1027 Fasen, K., Cerretti, D.P., and Huynh-Do, U. (2008). Ligand binding induces Cbl-dependent EphB1 receptor
1028 degradation through the lysosomal pathway. Traffic *9*, 251-266.

1029 Fawal, M.-A., Jungas, T., Kischel, A., Audouard, C., Iacovoni, J.S., and Davy, A. (2018). Cross Talk between
1030 One-Carbon Metabolism, Eph Signaling, and Histone Methylation Promotes Neural Stem Cell
1031 Differentiation. Cell Reports *23*, 2864-2873.e2867.

1032 Foot, N., Henshall, T., and Kumar, S. (2017). Ubiquitination and the Regulation of Membrane Proteins.
1033 Physiol Rev *97*, 253-281.

1034 Gagne, L.M., Morin, N., Lavoie, N., Bisson, N., Lambert, J.P., Mallette, F.A., and Huot, M.E. (2021).
1035 Tyrosine phosphorylation of DEPTOR functions as a molecular switch to activate mTOR signaling. J Biol
1036 Chem *297*, 101291.

1037 Gale, N.W., Holland, S.J., Valenzuela, D.M., Flenniken, A., Pan, L., Ryan, T.E., Henkemeyer, M., Strebhardt,
1038 K., Hirai, H., Wilkinson, D.G.*, et al.* (1996). Eph receptors and ligands comprise two major specificity
1039 subclasses and are reciprocally compartmentalized during embryogenesis. Neuron *17*, 9-19.

1040 Genander, M., Halford, M.M., Xu, N.-J., Eriksson, M., Yu, Z., Qiu, Z., Martling, A., Greicius, G., Thakar, S.,
1041 Catchpole, T.*, et al.* (2009). Dissociation of EphB2 signaling pathways mediating progenitor cell
1042 proliferation and tumor suppression. Cell *139*, 679-692.

1043 Grill, B., Bienvenut, W.V., Brown, H.M., Ackley, B.D., Quadroni, M., and Jin, Y. (2007). C. elegans RPM-1
1044 regulates axon termination and synaptogenesis through the Rab GEF GLO-4 and the Rab GTPase GLO-1.
1045 Neuron *55*, 587-601.

1046 Grill, B., Murphey, R.K., and Borgen, M.A. (2016). The PHR proteins: intracellular signaling hubs in
1047 neuronal development and axon degeneration. Neural development *11*, 8-18.

1048 Guo, Q., Xie, J., Dang, C.V., Liu, E.T., and Bishop, J.M. (1998). Identification of a large Myc-binding protein
1049 that contains RCC1-like repeats. Proc Natl Acad Sci U S A *95*, 9172-9177.

1050 Haglund, K., and Dikic, I. (2012). The role of ubiquitylation in receptor endocytosis and endosomal sorting.
1051 J Cell Sci *125*, 265-275.

1052 Hamburger, V., and Hamilton, H.L. (1951). A series of normal stages in the development of the chick
1053 embryo. J Morphol *88*, 49-92.

1054 Han, S., Kim, S., Bahl, S., Li, L., Burande, C.F., Smith, N., James, M., Beauchamp, R.L., Bhide, P., DiAntonio,
1055 A.*, et al.* (2012). The E3 ubiquitin ligase protein associated with Myc (Pam) regulates
1056 mammalian/mechanistic target of rapamycin complex 1 (mTORC1) signaling in vivo through N- and C-
1057 terminal domains. J Biol Chem *287*, 30063-30072.

1058 Henkemeyer, M., Orioli, D., Henderson, J.T., Saxton, T.M., Roder, J., Pawson, T., and Klein, R. (1996). Nuk
1059 controls pathfinding of commissural axons in the mammalian central nervous system. Cell *86*, 35-46.

1060 Huttlin, E.L., Bruckner, R.J., Navarrete-Perea, J., Cannon, J.R., Baltier, K., Gebreab, F., Gygi, M.P.,
1061 Thornock, A., Zarraga, G., Tam, S.*, et al.* (2021). Dual proteome-scale networks reveal cell-specific
1062 remodeling of the human interactome. Cell *184*, 3022-3040 e3028.

1063 Kania, A., and Klein, R. (2016). Mechanisms of ephrin-Eph signalling in development, physiology and
1064 disease. Nature reviews Molecular cell biology *17*, 240-256.

1065 Knight, J.D.R., Choi, H., Gupta, G.D., Pelletier, L., Raught, B., Nesvizhskii, A.I., and Gingras, A.C. (2017).
1066 ProHits-viz: a suite of web tools for visualizing interaction proteomics data. Nat Methods *14*, 645-646.

1067 Kullander, K., Mather, N.K., Diella, F., Dottori, M., Boyd, A.W., and Klein, R. (2001). Kinase-dependent
1068 and kinase-independent functions of EphA4 receptors in major axon tract formation in vivo. Neuron *29*,
1069 73-84.

1070 Lackmann, M., Oates, A.C., Dottori, M., Smith, F.M., Do, C., Power, M., Kravets, L., and Boyd, A.W. (1998).
1071 Distinct subdomains of the EphA3 receptor mediate ligand binding and receptor dimerization. J Biol
1072 Chem *273*, 20228-20237.

1073 Lahaie, S., Morales, D., Bagci, H., Hamoud, N., Castonguay, C.-E., Kazan, J.M., Desrochers, G., Klar, A.,
1074 Gingras, A.-C., Pause, A.*, et al.* (2019). The endosomal sorting adaptor HD-PTP is required for ephrin-
1075 B:EphB signalling in cellular collapse and spinal motor axon guidance. Scientific reports *9*, 11945.

1076 Lewcock, J.W., Genoud, N., Lettieri, K., and Pfaff, S.L. (2007). The Ubiquitin Ligase Phr1 Regulates Axon
1077 Outgrowth through Modulation of Microtubule Dynamics. Neuron *56*, 604-620.

1078 Litterst, C., Georgakopoulos, A., Shioi, J., Ghersi, E., Wisniewski, T., Wang, R., Ludwig, A., and Robakis,
1079 N.K. (2007). Ligand binding and calcium influx induce distinct ectodomain/gamma-secretase-processing
1080 pathways of EphB2 receptor. J Biol Chem *282*, 16155-16163.

1081 Liu, G., Zhang, J., Larsen, B., Stark, C., Breitkreutz, A., Lin, Z.Y., Breitkreutz, B.J., Ding, Y., Colwill, K.,
1082 Pasculescu, A*., et al.* (2010). ProHits: integrated software for mass spectrometry-based interaction
1083 proteomics. Nat Biotechnol *28*, 1015-1017.

1084 Luria, V., Krawchuk, D., Jessell, T.M., Laufer, E., and Kania, A. (2008). Specification of motor axon
1085 trajectory by ephrin-B:EphB signaling: symmetrical control of axonal patterning in the developing limb.
1086 Neuron *60*, 1039-1053.

1087 Margolis, S.S., Salogiannis, J., Lipton, D.M., Mandel-Brehm, C., Wills, Z.P., Mardinly, A.R., Hu, L., Greer,
1088 P.L., Bikoff, J.B., Ho, H.Y*., et al.* (2010). EphB-mediated degradation of the RhoA GEF Ephexin5 relieves a
1089 developmental brake on excitatory synapse formation. Cell *143*, 442-455.

1090 Mellitzer, G., Xu, Q., and Wilkinson, D.G. (1999). Eph receptors and ephrins restrict cell intermingling and
1091 communication. Nature *400*, 77-81.

1092 Mohamed, A.M., and Chin-Sang, I.D. (2006). Characterization of loss-of-function and gain-of-function
1093 Eph receptor tyrosine kinase signaling in C. elegans axon targeting and cell migration. Dev Biol *290*, 164-
1094 176.

1095 Na, Y., Calvo-Jimenez, E., Kon, E., Cao, H., Jossin, Y., and Cooper, J.A. (2020). Fbxo45 Binds SPRY Motifs
1096 in the Extracellular Domain of N-Cadherin and Regulates Neuron Migration during Brain Development.
1097 Mol Cell Biol *40*.

1098 Nakata, K., Abrams, B., Grill, B., Goncharov, A., Huang, X., Chisholm, A.D., and Jin, Y. (2005). Regulation
1099 of a DLK-1 and p38 MAP kinase pathway by the ubiquitin ligase RPM-1 is required for presynaptic
1100 development. Cell *120*, 407-420.

1101 Nie, D., Di Nardo, A., Han, J.M., Baharanyi, H., Kramvis, I., Huynh, T., Dabora, S., Codeluppi, S., Pandolfi,
1102 P.P., Pasquale, E.B*., et al.* (2010). Tsc2-Rheb signaling regulates EphA-mediated axon guidance. Nature
1103 Neuroscience *13*, 163-172.

1104 Okumura, F., Joo-Okumura, A., Obara, K., Petersen, A., Nishikimi, A., Fukui, Y., Nakatsukasa, K., and
1105 Kamura, T. (2017). Ubiquitin ligase SPSB4 diminishes cell repulsive responses mediated by EphB2.
1106 Molecular biology of the cell *28*, 3532-3541.

1107 Pao, K.C., Wood, N.T., Knebel, A., Rafie, K., Stanley, M., Mabbitt, P.D., Sundaramoorthy, R., Hofmann, K.,
1108 van Aalten, D.M.F., and Virdee, S. (2018). Activity-based E3 ligase profiling uncovers an E3 ligase with
1109 esterification activity. Nature *556*, 381-385.

1110 Perez-Riverol, Y., Csordas, A., Bai, J., Bernal-Llinares, M., Hewapathirana, S., Kundu, D.J., Inuganti, A.,
1111 Griss, J., Mayer, G., Eisenacher, M*., et al.* (2019). The PRIDE database and related tools and resources in
1112 2019: improving support for quantification data. Nucleic Acids Res *47*, D442-D450.

1113 Poliak, S., Morales, D., Croteau, L.-P., Krawchuk, D., Palmesino, E., Morton, S., Jean-François, C., Charron,
1114 F., Dalva, M.B., Ackerman, S.L.*, et al.* (2015). Synergistic integration of Netrin and ephrin axon guidance
1115 signals by spinal motor neurons. eLife *4*, e10841.

1116 Poliakov, A., Cotrina, M.L., Pasini, A., and Wilkinson, D.G. (2008). Regulation of EphB2 activation and cell
1117 repulsion by feedback control of the MAPK pathway. The Journal of cell biology *183*, 933-947.

1118 Sabet, O., Stockert, R., Xouri, G., Bruggemann, Y., Stanoev, A., and Bastiaens, P.I.H. (2015). Ubiquitination
1119 switches EphA2 vesicular traffic from a continuous safeguard to a finite signalling mode. Nat Commun *6*,
1120 8047.

1121 Saiga, T., Fukuda, T., Matsumoto, M., Tada, H., Okano, H.J., Okano, H., and Nakayama, K.I. (2009). Fbxo45
1122 forms a novel ubiquitin ligase complex and is required for neuronal development. Molecular and Cellular
1123 Biology *29*, 3529-3543.

1124 Salokas, K., Liu, X., Ohman, T., Chowdhury, I., Gawriyski, L., Keskitalo, S., and Varjosalo, M. (2022).
1125 Physical and functional interactome atlas of human receptor tyrosine kinases. EMBO Rep *23*, e54041.

1126 Schaupp, A., Sabet, O., Dudanova, I., Ponserre, M., Bastiaens, P., and Klein, R. (2014). The composition
1127 of EphB2 clusters determines the strength in the cellular repulsion response. J Cell Biol *204*, 409-422.

1128 Schindelin, J., Arganda-Carreras, I., Frise, E., Kaynig, V., Longair, M., Pietzsch, T., Preibisch, S., Rueden, C.,
1129 Saalfeld, S., Schmid, B.*, et al.* (2012). Fiji: an open-source platform for biological-image analysis. Nat
1130 Methods *9*, 676-682.

1131 Sharfe, N., Freywald, A., Toro, A., and Roifman, C.M. (2003). Ephrin-A1 induces c-Cbl phosphorylation
1132 and EphA receptor down-regulation in T cells. J Immunol *170*, 6024-6032.

1133 Sharma, J., Baker, S.T., Turgeon, S.M., Gurney, A.M., Opperman, K.J., and Grill, B. (2014). Identification
1134 of a peptide inhibitor of the RPM-1 . FSN-1 ubiquitin ligase complex. J Biol Chem *289*, 34654-34666.

1135 Shi, L., Fu, W.Y., Hung, K.W., Porchetta, C., Hall, C., Fu, A.K., and Ip, N.Y. (2007). Alpha2-chimaerin
1136 interacts with EphA4 and regulates EphA4-dependent growth cone collapse. Proc Natl Acad Sci U S A *104*,
1137 16347-16352.

1138 Soskis, M.J., Ho, H.Y., Bloodgood, B.L., Robichaux, M.A., Malik, A.N., Ataman, B., Rubin, A.A., Zieg, J.,
1139 Zhang, C., Shokat, K.M.*, et al.* (2012). A chemical genetic approach reveals distinct EphB signaling
1140 mechanisms during brain development. Nat Neurosci *15*, 1645-1654.

1141 Srivastava, N., Robichaux, M.A., Chenaux, G., Henkemeyer, M., and Cowan, C.W. (2013). EphB2 receptor
1142 forward signaling controls cortical growth cone collapse via Nck and Pak. Mol Cell Neurosci *52*, 106-116.

1143 Teo, G., Liu, G., Zhang, J., Nesvizhskii, A.I., Gingras, A.C., and Choi, H. (2014). SAINTexpress:
1144 improvements and additional features in Significance Analysis of INTeractome software. J Proteomics
1145 *100*, 37-43.

1146 Venkitachalam, S., Babu, D., Ravillah, D., Katabathula, R.M., Joseph, P., Singh, S., Udhayakumar, B., Miao,
1147 Y., Martinez-Uribe, O., Hogue, J.A.*, et al.* (2022). The Ephrin B2 Receptor Tyrosine Kinase Is a Regulator
1148 of Proto-oncogene MYC and Molecular Programs Central to Barrett's Neoplasia. Gastroenterology *163*,
1149 1228-1241.

1150 Virdee, S. (2022). An atypical ubiquitin ligase at the heart of neural development and programmed axon
1151 degeneration. Neural Regen Res *17*, 2347-2350.

1152 Walker-Daniels, J., Riese, D.J., 2nd, and Kinch, M.S. (2002). c-Cbl-dependent EphA2 protein degradation
1153 is induced by ligand binding. Mol Cancer Res *1*, 79-87.

1154 Wan, H.I., DiAntonio, A., Fetter, R.D., Bergstrom, K., Strauss, R., and Goodman, C.S. (2000). Highwire
1155 regulates synaptic growth in Drosophila. Neuron *26*, 313-329.

1156 Williams, S.E., Mann, F., Erskine, L., Sakurai, T., Wei, S., Rossi, D.J., Gale, N.W., Holt, C.E., Mason, C.A.,
1157 and Henkemeyer, M. (2003). Ephrin-B2 and EphB1 mediate retinal axon divergence at the optic chiasm.
1158 Neuron *39*, 919-935.

1159 Xiong, X., Hao, Y., Sun, K., Li, J., Li, X., Mishra, B., Soppina, P., Wu, C., Hume, R.I., and Collins, C.A. (2012).
1160 The Highwire ubiquitin ligase promotes axonal degeneration by tuning levels of Nmnat protein. PLoS Biol
1161 *10*, e1001440.

1162 Zhen, M., Huang, X., Bamber, B., and Jin, Y. (2000). Regulation of presynaptic terminal organization by C.
1163 elegans RPM-1, a putative guanine nucleotide exchanger with a RING-H2 finger domain. Neuron *26*, 331-
1164 343.

1165 Zimmer, M., Palmer, A., Köhler, J., and Klein, R. (2003). EphB-ephrinB bi-directional endocytosis
1166 terminates adhesion allowing contact mediated repulsion. Nature Cell Biology *5*, 869-878.
1167